ERCB/AGS Open File Report 2009-03

ERCB

Geochemical and Petrographic Evaluation of Downhole Gamma-Ray Anomalies in the Buffalo Head Hills Kimberlite Field, North-Central Alberta (NTS 84B/13)

Energy Resources Conservation Board

AGS
Alberta Geological Survey

ERCB/AGS Open File Report 2009-03

Geochemical and Petrographic Evaluation of Downhole Gamma-Ray Anomalies in the Buffalo Head Hills Kimberlite Field, North-Central Alberta (NTS 84B/13)

D.R. Eccles

Energy Resources Conservation Board
Alberta Geological Survey

March 2009

ISBN 978-0-7785-6973-2

When using information from this publication in other publications or presentations, due acknowledgment should be given to the ERCB/AGS. The following reference format is recommended:

Eccles, D.R. (2009): Geochemical and petrographic evaluation of downhole gamma-ray anomalies in the Buffalo Head Hills kimberlite field, north-central Alberta (NTS 84B/13); Energy Resources Conservation Board, ERCB/AGS Open File Report 2009-03, 23 p.

Published March 2009 by:
Energy Resources Conservation Board
Alberta Geological Survey
4th Floor, Twin Atria Building
4999 – 98th Avenue
Edmonton, Alberta
T6B 2X3
Canada

Tel: 780.422.3767
Fax: 780.422.1918
E-mail: AGS-Info@ercb.ca
Website: www.ags.gov.ab.ca

Contents

Acknowledgments.......v
Abstract.......vi
1 Introduction.......1
2 Drillhole BHH04-KHR-02.......1
3 Analytical Methodology.......3
4 Geochemical Results.......3
4.1 Whole-Rock Geochemical Observations Associated with the K-log Geophysical Anomaly.......3
4.2 Whole-Rock Geochemical and Petrographic Observations Associated with the U-Log Geophysical Anomaly.......5
4.3 Whole-Rock Geochemical Observations Associated with the Th-log Geophysical Anomaly.......10
5 Conclusion.......12
6 References.......13
Appendices.......14
Appendix 1. Major and Trace-Element Whole-Rock Geochemistry of Selected Samples from Drillhole BHH04-KHR-02.......14
Appendix 2. X-Ray Diffractogram for Selected Samples from Drillhole BHH04-KHR-02.......18

Tables

Table 1. Description of core samples with elevated K_2O, U and Th, drillhole BHH04-KHR-02.......5
Table 2. Modal mineral composition of sample L146.......8
Table 3. Selected geochemical data for the Th-log gamma-ray anomaly samples L150 and L151, with the average composition of the remaining sedimentary rock samples analyzed in this study and Buffalo Head Hills kimberlite compositions for comparison.......11

Figures

Figure 1. Geological setting of the northern Alberta kimberlite province and the location of stratigraphic hole BHH04-KHR-2, drilled to study uppermost Late Cretaceous and Paleocene sedimentary rocks in north-central Alberta.......2
Figure 2. Gamma-ray logs from drillhole BHH04-KHR-2.......4
Figure 3. Chondrite-normalized (a) and North American shale composite (NASC)–normalized (b) rare-earth element plots for selected samples from drillhole BHH04-KHR-02.......6
Figure 4. Clustered column diagrams comparing Th, U and total organic carbon from drillhole BHH04-KHR-02 core samples with U- and Th-logs.......7
Figure 5. Photomicrographs of sample L146.......9
Figure 6. Uranium versus total organic carbon for samples from drillhole BHH04-KHR-02.......10

Acknowledgments

I wish to acknowledge J. Mwenifumbo and B. Hyatt of the Geological Survey of Canada for their contribution in field-data acquisition and discussion. The drilling and downhole geophysics were part of the 2003–2007 Northern Resource Development (NRD) joint initiative between the federal and Alberta governments. A.P. Beaton of Alberta Geological Survey is thanked for his review of the report.

Abstract

Core from a stratigraphic study drillhole, which was collared adjacent to the K4B kimberlite in the Buffalo Head Hills field of north-central Alberta, was tested by downhole gamma-ray geophysics, whole-rock geochemistry and petrography. A combined uranium- and thorium-log gamma-ray anomaly and a coincident kimberlite geochemical affinity suggest that sedimentary rocks cored at this horizon have been augmented either by syndepositional kimberlite volcanism or by kimberlitic fluids moving intrusively through the sedimentary strata. In contrast, a uranium-log gamma-ray anomaly coinciding with elevated total organic carbon and sulphide- and hematite-replaced organic material suggests reduction and accumulation of uranium and other metallic minerals and pathfinder elements (Mo, Zn, Ba, Hg, Sb, Se) as fluids moved through an organic-rich sedimentary rock horizon.

These observations are particularly important when the more than 500 000 oil and gas exploration wells drilled in the Western Canadian Sedimentary Basin are considered. Interpretation and correlation of analytical techniques, such as those presented in this study, may lead to methods that utilize wireline-log information to assess the regional potential for diamondiferous kimberlite and metalliferous deposits in Alberta.

1 Introduction

During December 2004, the Geological Survey of Canada (GSC) and the Alberta Geological Survey (AGS) drilled a stratigraphic study hole, BHH04-KHR-2, in the Buffalo Head Hills kimberlite field of north-central Alberta to obtain uppermost Late Cretaceous and Paleocene sedimentary cores (Figure 1). The drillhole, which was collared approximately 500 m west of the K4B kimberlite, cored more than 90 m of continuous bedrock. The primary objective for the study drillhole was to obtain rocks that were previously inaccessible because the area is covered by surficial deposits of variable thickness, and the uppermost sedimentary rock strata are typically not recovered during oil and gas exploration. A second objective was to core a sedimentary rock section adjacent to a known kimberlite body, in order to study sedimentary rock characteristics in a 'proximal' kimberlite setting. A third objective was to log the drillhole by borehole natural gamma-ray (γ-ray) measurements, which can be useful in mapping relatively unknown strata.

Calcareous, competent, bluish grey cores that resemble kimberlite were observed during drilling. Because these anomalous core intersections appear to correlate with downhole geophysical γ-ray spikes, the purpose of this study is to report on the geochemical and petrographic characteristics of the cores that occur at the same depths as the downhole geophysical γ-ray anomalies. These observations are particularly important considering that more than 500 000 oil and gas exploration wells with wireline logs have been drilled in the Western Canadian Sedimentary Basin (WCSB). If the geophysical anomalies documented here are related to kimberlite, then this might provide a new technique to aid in the discovery of unknown occurrences of kimberlite in the WCSB.

2 Drillhole BHH04-KHR-02

The BBH04-KHR-2 drill site is located on the north side of the Sawn Lake Battery road, approximately 33 km west of its junction with Highway 88. A cutline was ploughed (snow removal) to a naturally cleared area approximately 150 m off the road. The drill was collared adjacent to the K4 kimberlite complex, approximately 500 m west of the centre of the K4B kimberlite, which is inferred from the ground geophysical survey of Skelton and Bursey (1998). The BBH04-KHR-2 drill site was selected because of its proximity to the K4B kimberlite (Figure 1) and because previous AGS core-auger studies showed that the area is covered by a relatively thin veneer of overburden (approximately 10 m; Pawlowicz et al., 2005).

Bedrock was intersected at a depth of 7.93 m and cored continuously to a depth of 105.16 m. The dominant lithology is grey to dark grey, massive mudstone with variable proportions of interbedded siltstone and sandstone (Figure 1). The depositional environment is interpreted as lower shoreface, offshore shelf, becoming more distal with depth (Hein and Eccles, 2007). Based on regional stratigraphic studies (Chen and Olson, 2005), the stratigraphic interval intersected in BBH04-KHR-2 most likely belongs to the Puskwaskau Formation of the upper Smoky Group. Palynological interpretations by Sweet et al. (Palynological constraints on kimberlite emplacement models: chronostratigraphy of host rock and clastic xenoliths, work in progress, 2009), however, indicate an abrupt change from Campanian to Santonian assemblages in the BBH04-KHR-2 mudstone succession that correlate with the Wapiti Group and the Puskwaskau Formation, respectively (contact at an approximate core depth of 82 m).

At the base of the drillcore, a coarser sandstone interval is stratigraphically too deep to belong to either the Cardium or Dunvegan formations, based on wireline-log correlations with surrounding oil and gas wells. Hein and Eccles (2007) suggested this sandstone unit may represent the older Paddy-Cadotte (Albian) succession, marking a major unconformity that separates the basal sandstone (Albian) from the overlying Santonian mudstone succession. This would mean that the total succession from late Albian to late Turonian is missing. However, Sweet et al. (work in progress, 2009) are currently validating the hypothesis of a Turonian to Santonian hiatus, in which case the basal sandstone in BBH04-KHR-2 could

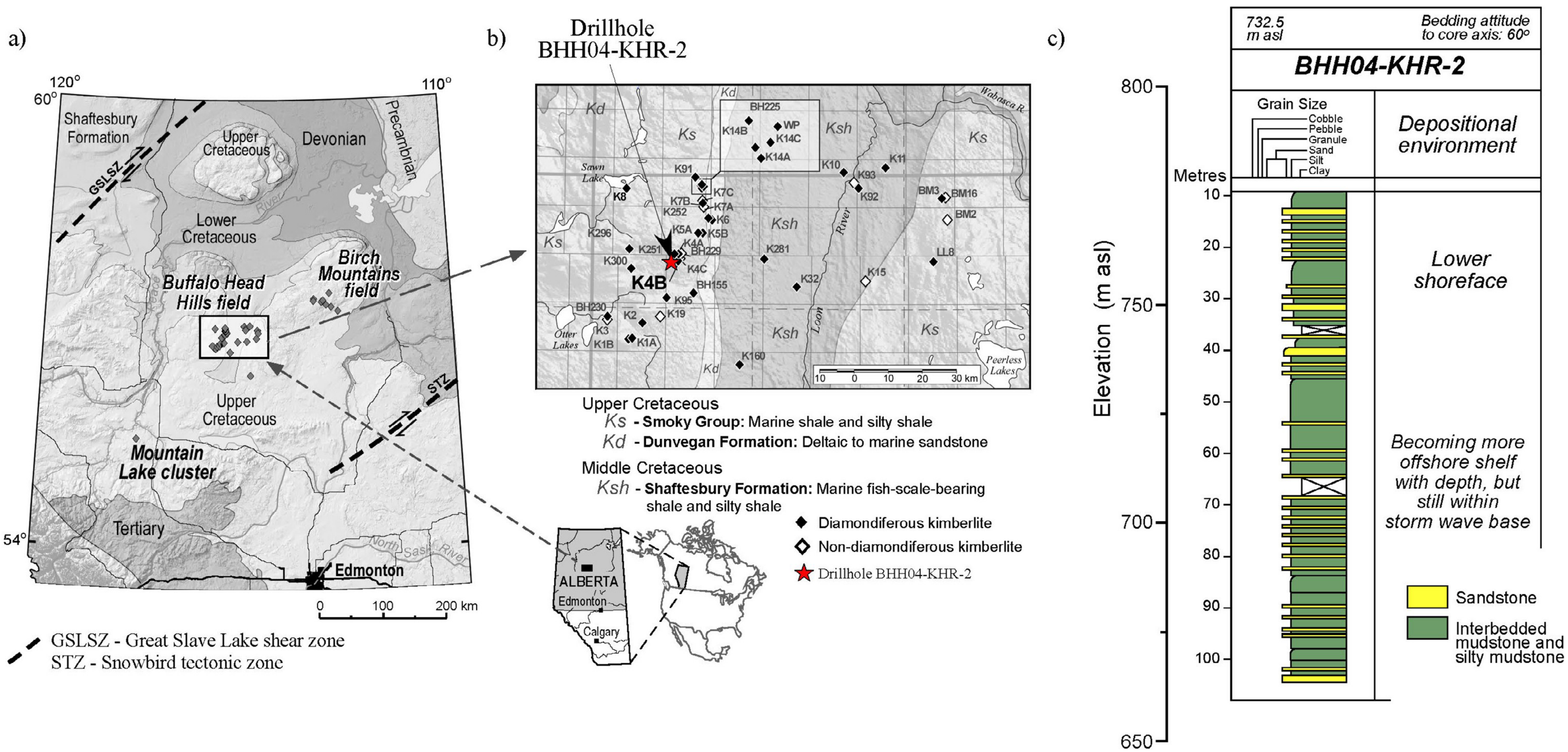

Figure 1. Geological setting of the northern Alberta kimberlite province and the location of stratigraphic hole BHH04-KHR-2, drilled to study uppermost Late Cretaceous and Paleocene sedimentary rocks in north-central Alberta: a) ultrabasic to kimberlite occurrences in the Mountain Lake, Buffalo Head Hills and Birch Mountains fields; b) locations of kimberlitic occurrences in the Buffalo Head Hills field and stratigraphic drillhole BHH04-KHR-2 (bedrock geology *simplified from* Hamilton et al., 1999); c) simplified drillcore log for BHH04-KHR-2 (*from* Hein and Eccles, 2008) to illustrate general rock types and depositional environment; datum is sea level.

belong to the Cenomanian Dunvegan Formation. Circulation for the drillhole was lost at approximately 104.73 m when coarse-grained, fractured sandstone was intersected. Several attempts to ‘blind drill’ (without circulation) through the sandstone failed and the hole was abandoned at a depth of 105.16 m.

3 Analytical Methodology

Following the methodology of Mwenifumbo and Kjarsgaard (1999), the GSC Research and Development logging system was used to acquire downhole γ-ray readings, which measure the natural γ-rays emitted by the potassium-40 (^{40}K), uranium (U) and thorium (Th) decay series nuclides in the rocks, and are presented in Figure 2. The total-count γ-ray log (Figure 2a) shows varying levels of radioactivity that likely correspond to changes in lithology. For example, increasing levels of radioactivity between 10 and 32 m are related to increases in clay content of mudstone (i.e., potassium enrichment), whereas low γ-ray levels (e.g., at 32 m) correspond to sandstone-dominated strata. The total-count γ-ray log is relatively homogeneous until 97–103 m, where there are distinct spikes associated with U- and Th-log anomalies (Figure 2b).

Thirty-two core samples were collected from drillhole BHH04-KHR-02. Analytical splits were sent to Acme Analytical Laboratories Ltd. (Vancouver, British Columbia) for the following sample preparation and analysis:

- crushing and pulverizing with mild steel and preservation of the +150 and –150 mesh fractions
- Group 4A whole-rock and Group 4B trace-element analysis by ICP: whole-rock by $LiBO_2$ fusion–dilute nitric digestion and inductively coupled plasma–emission spectroscopy (ICP-ES); rare-earth elements by $LIBO_2$ fusion and inductively couple plasma–mass spectrometry (ICP-MS); and precious and base metals by aqua regia digestion and ICP-MS; this package includes loss-on-ignition and carbon and sulphur by Leco
- Group 1EX four-acid digestion: a 0.25 g split is heated in HNO_3-$HClO_4$-HF to fuming and taken to dryness; the residue is dissolved in HCl and the solutions are analyzed by ICP-MS
- Group 1F-MS with Pt, Pd: ICP-MS analysis of a 15 g sample after aqua regia digestion

Analytical results included quality-control samples inserted by Acme (standards and silica blanks) and Canadian Certified Reference Materials SY-4 (diorite gneiss) and WGB-1 (gabbro) inserted by the author.

Samples for analysis by the X-ray diffraction standard powder method were prepared at the Alberta Geological Survey laboratory by grinding to <125 µm with a ceramic mortar/pestle and then analyzed at the University of Alberta using a Rigaku Geigerflex powder diffractometer with a Co tube and graphite monochromator.

4 Geochemical Results

Geochemical and X-ray data are presented in Appendices 1 and 2, respectively. The K, U and Th downhole γ-ray anomalies from BHH04-KHR-02 occur at the same core depths as whole-rock geochemical data with elevated K_2O, U and Th compositions. The anomalous samples are summarized in Table 1 and discussed below.

4.1 Whole-Rock Geochemical Observations Associated with the K-log Geophysical Anomaly

The K-log shows a fairly uniform level of radioactivity of approximately 4–8 counts per second (cps), with slightly higher radioactivity between 96 and 98 m, and at 102 m (Figure 2). Samples L140–L142, obtained from between 95.11 and 98.20 m, occur at the same depth as the most significant K-log anomaly. Rocks at this horizon are dominated by dark grey marine mudstone with K_2O concentrations of 3.24%–3.36%, values that are slightly to moderately elevated with respect to all other BBH04-KHR-02

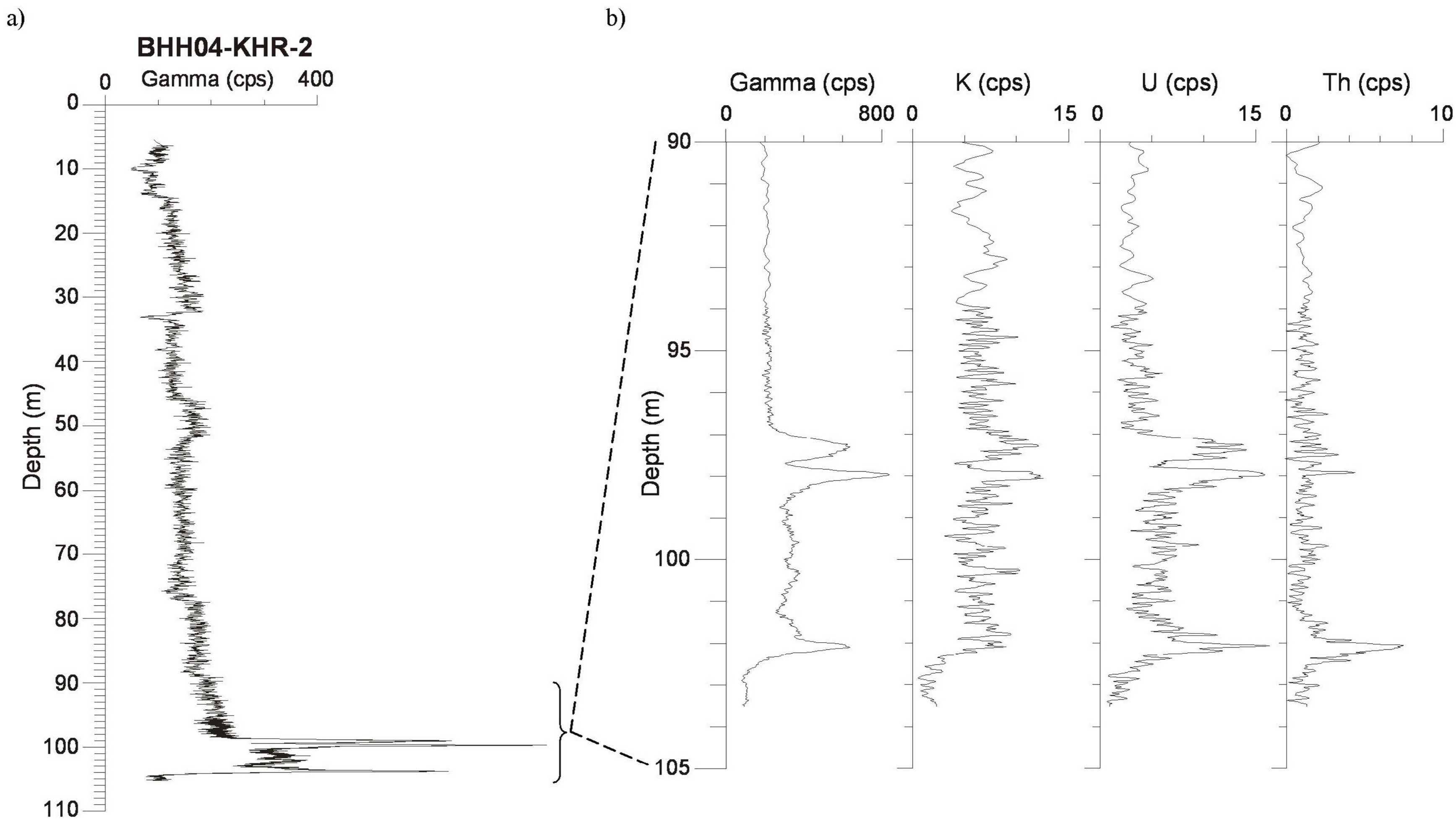

Figure 2. Gamma-ray logs from drillhole BHH04-KHR-2: a) total-count gamma-ray log; b) unprocessed spectral gamma-ray logs for total count, K, U and Th from a depth of 90–105 m.

core samples. Chondrite- and North American shale composite (NASC)–normalized rare-earth element (REE) patterns on Figure 3 show a generally flat trend with slightly negative and positive Eu anomalies, respectively. The K_2O-rich mudstone has the highest REE abundance relative to mudstone from BHH04-KHR-02 and to mudstone from the previous studies in the Buffalo Head Hills area (Figure 3).

Table 1. Description of core samples with elevated K_2O, U and Th, drillhole BHH04-KHR-02.

Sample ID	Geophysical Spike *	Drillhole ID	Sample Top (m)	Sample Bottom (m)	Elevation (m asl)	Lithology
RE05-KHR-L140	K_2O	BHH04-KHR-2	95.11	95.50	682	Dark grey mudstone (note: core problems)
RE05-KHR-L141	K_2O	BHH04-KHR-2	96.01	96.50	681	Grey, blocky mudstone
RE05-KHR-L142	K_2O	BHH04-KHR-2	97.54	98.20	679	Grey mudstone at transition to organic-rich black mudstone
RE05-KHR-L146	U spike	BHH04-KHR-2	99.00	99.06	678	Interbedded carbonate-enriched sandstone and bituminous mudstone
RE05-KHR-L150	Th spike	BHH04-KHR-2	103.41	103.46	674	Silty mudstone with white Fe-sulphates
RE05-KHR-L151	Th spike	BHH04-KHR-2	103.55	103.60	673	Coarse-grained, Fe-stained sandstone (regolith appearance)

* Based on downhole geophysical gamma measurements

An unequivocal explanation for these elevated K_2O concentrations in the mudstone is not known. Commonly, the K content in mudstone correlates with clay minerals and, more specifically, Al silicates. X-ray diffraction analysis on this suite of samples shows the presence of chlorite group minerals (clinochlore and nimite; Appendix 2), which could account for an increased modal abundance of Al-silicate clay minerals and therefore the K-log anomaly.

Alternatively, several interesting coincidences are provided below. First, the K_2O-rich mudstone has a positive Eu anomaly with respect to the NASC-normalized REE (Figure 3B). The positive Eu anomaly was not observed in the regional suite of Buffalo Head Hills mudstone analyzed by Dufresne et al. (2001), so the Eu anomaly in samples L140–L142 could have resulted from a zone of localized hydrothermal activity (e.g., Michard and Albarede, 1986; Klinkhammer et al., 1994; Mills and Elderfield, 1995). Secondly, the elevation of the K_2O-rich mudstone (679–682 m asl) is approximately the same as that of an andesite tuff horizon that was recently discovered in two drillholes (DDH-296-03 and -300-01) located approximately 15–18 km west of BBH04-KHR-02 (Eccles, unpublished data, 2008). The andesite tuff has high anorthite content ($An_{40–47}$). X-ray diffraction shows the mudstone samples associated with the K-log anomaly to include quartz, muscovite, anorthite, wollastonite and clinochlore (Appendix 2). The presence of anorthite, in particular, could provide evidence that intermediate volcanic rocks have influenced the mudstone.

To summarize, given the number of scenarios presented above, it is possible that the K-log anomaly could reflect a combination of proximal to distal sources and/or influences.

4.2 Whole-Rock Geochemical and Petrographic Observations Associated with the U-Log Geophysical Anomaly

Samples L143 and L146, which were obtained from depths of 98.2 and 99.0 m, have the highest U concentrations (37.8 and 83.2 ppm, respectively) in the set of BHH04-KHR-02 core samples. Of particular interest is sample L146, which best correlates with the U-log anomaly (Figure 4). This sample is a carbonate (ankerite)– and pyrite-enriched silty sandstone with the modal mineral composition shown in Table 2.

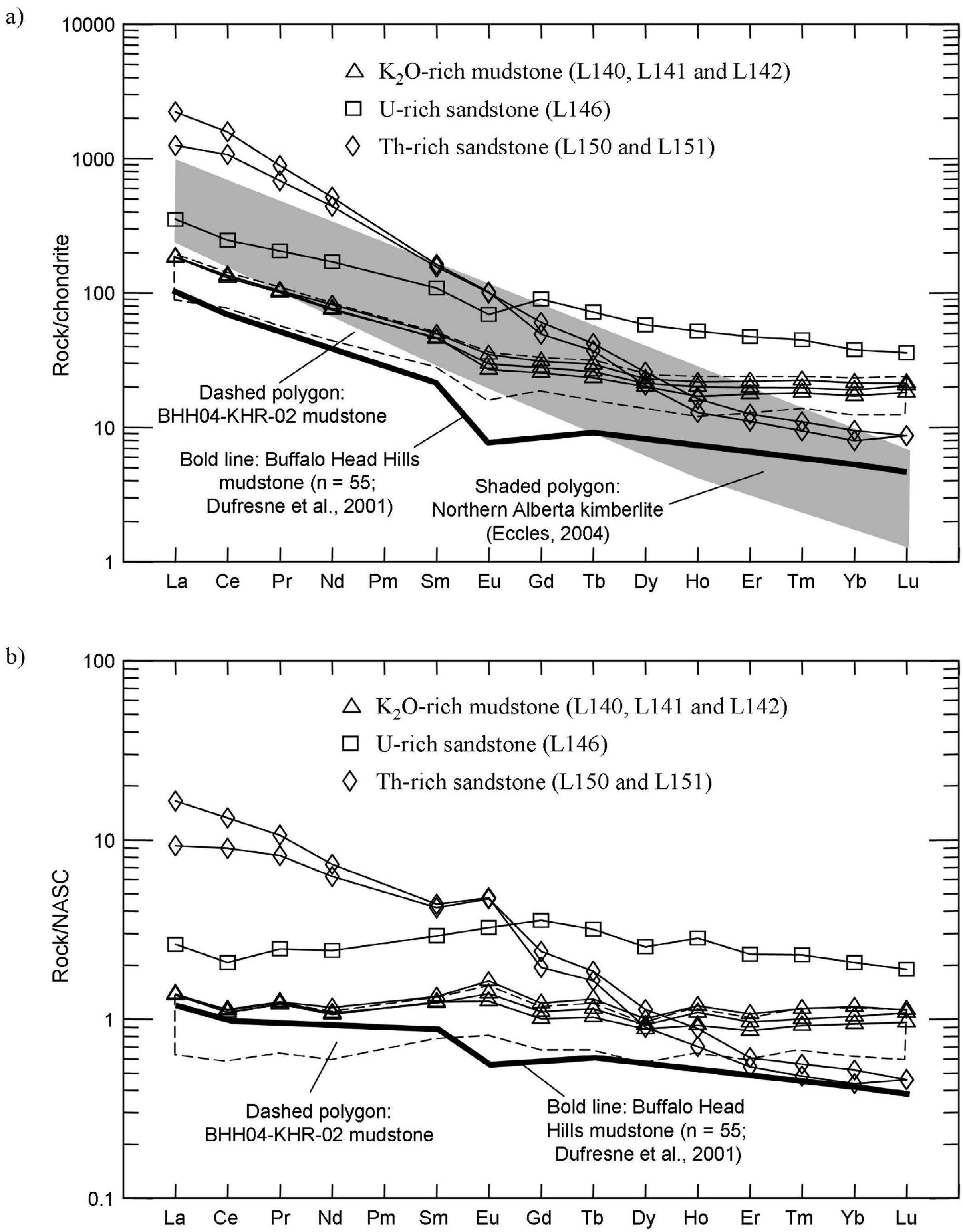

Figure 3. Chondrite-normalized (a) and North American shale composite (NASC)–normalized (b) rare-earth element plots for selected samples from drillhole BHH04-KHR-02 to make comparisons between the K_2O-, U- and Th-rich mudstone and sandstone discussed in this study versus ultramafic rocks from the northern Alberta kimberlite field and mudstone from the Buffalo Head Hills and drillhole BHH04-KHR-02; chondrite values from Sun and McDonough (1989) and NASC values from Gromet et al. (1984).

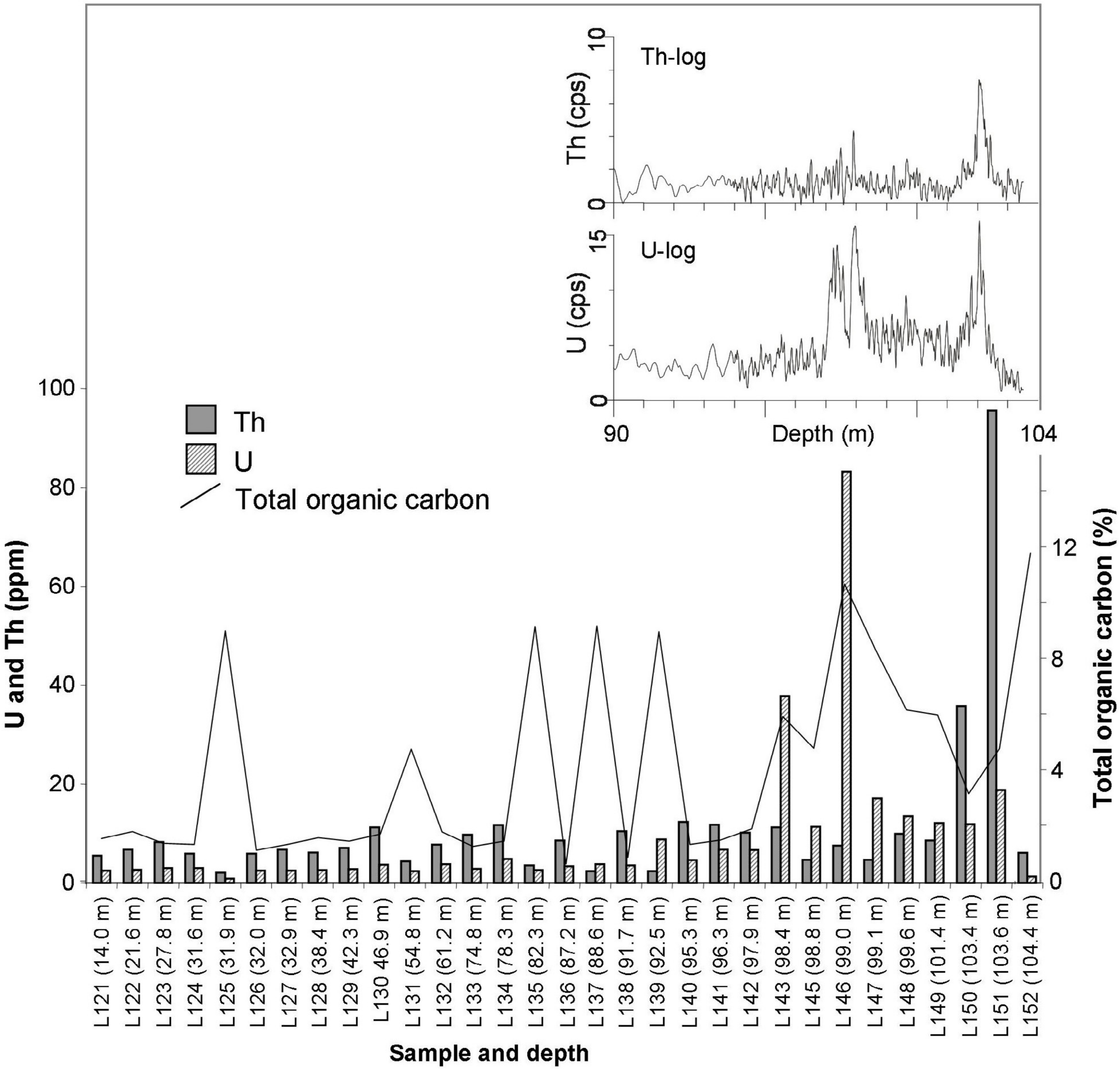

Figure 4. Clustered column diagrams comparing Th, U and total organic carbon from drillhole BHH04-KHR-02 core samples with U- and Th-logs (*from* Figure 2).

Sample L146 is moderately banded. These bands are distinguished by variations in the abundance of detrital grains versus ankerite and pyrite (Figure 5). Banded variations include the following:

- Band A contains abundant ankerite, is stained medium brown by limonite and contains about 2% disseminated pyrite (0.003–0.01 mm; Figure 5a). Quartz and biotite form minor detrital grains up to 0.1 mm in size. Biotite is pleochroic from light to dark brown. Nonreflective opaque minerals form wispy lenses up to 0.6 mm long and parallel to banding. Bright red hematite forms a few irregular, interstitial patches.

Table 2. Modal mineral composition of sample L146.

Mineral	Percentage	Main Grain-Size Range (mm)
Ankerite	85–87	0.02–0.05
Pyrite	5–7	0.003–0.05
Quartz	4–5	0.03–0.07
Biotite	2–3	0.1–0.5
Plagioclase	0.5	0.05–0.1
Muscovite	0.2	0.05–0.1
Hematite	0.1	amorphous
Ilmenite	minor	0.03–0.05

- Band B is an ankeritic siltstone that contains moderately (5%–7%) abundant detrital grains of quartz and 3%–4% detrital flakes of biotite in a matrix of ankerite with minor disseminated pyrite. Biotite flakes are oriented parallel to compositional banding and are pleochroic, as in band A. Pyrite forms 3%–5% disseminated patches up to 0.07 mm in size.
- Band C is gradational from band B, with detrital grains of quartz and biotite in a groundmass dominated by pyrite with minor ankerite (Figure 5b).
- Band D is dominated by ankerite with disseminated patches of nonreflective opaque minerals and minor detrital grains of quartz. Ankerite is banded moderately parallel to compositional banding.
- Band E is dominated by pyrite with minor detrital grains of quartz (0.02–0.05 mm). Towards the end of this band, pyrite becomes much less abundant and in its place is a nonreflective opaque mineral containing minor pyrite.
- Band F is intermediate in composition between Bands A and B, with 3%–5% detrital grains of quartz and 2%–3% slender biotite flakes in a groundmass of ankerite. Pyrite forms 3%–5% disseminated patches up to 0.07 mm in size. Ilmenite forms minor, rounded to subhedral, platy grains. The contact between Bands and G is gradational.
- Band G is a slightly ankeritic, silty mudstone containing minor (2%–3%) detrital grains of quartz, minor biotite and lenses parallel to foliation of nonreflective and reddish brown hematite in a cryptocrystalline groundmass of uncertain composition containing scattered grains of ankerite (Figure 5c). Pyrite is concentrated moderately to strongly in diffuse lenses parallel to foliation.

This banding, which is characterized by variable amounts of carbonate- and/or pyrite-rich material, provides evidence of fluid movement and carbonate-sulphide accumulation in these silty sandstone sedimentary rock layers. In addition, the abundance of organic debris and evidence of organic material replacement by sulphide and hematite suggest mineralization in a reducing environment.

Geochemically, sample L146 is anomalous compared to all other BHH04-KHR-02 core samples and contains the highest concentrations of U (83 ppm), Ba (7366 ppm), Mo (159 ppm), Zn (388 ppm), Cd (10 ppm), Sb (11 ppm), Hg (143 ppb) and Se (31 ppm). Figure 4 shows that the U anomaly in sample L146 correlates well with a horizon of high total organic carbon (TOC). This can also be shown on the plot of U versus TOC, where sample L146 has high U and TOC relative to all other samples discussed in this report (Figure 6). This observation, together with high Cd, which is common in bone bed units in northern Alberta, provide further evidence that the trace metals, including U, are associated with an organic-rich (i.e., reducing) sedimentary environment.

a)

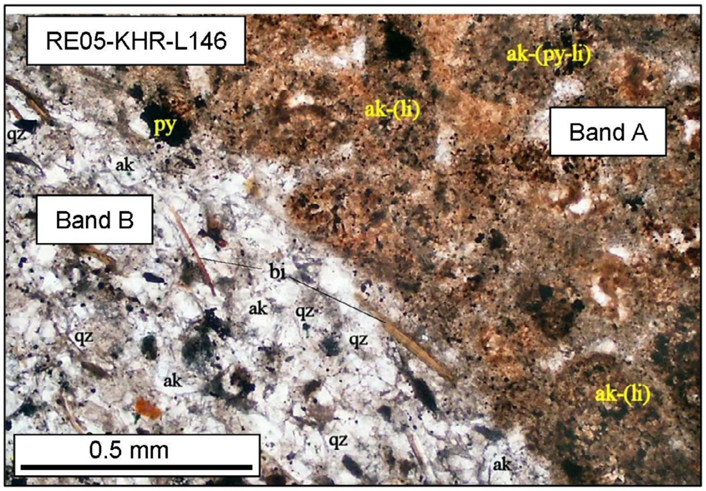

b)

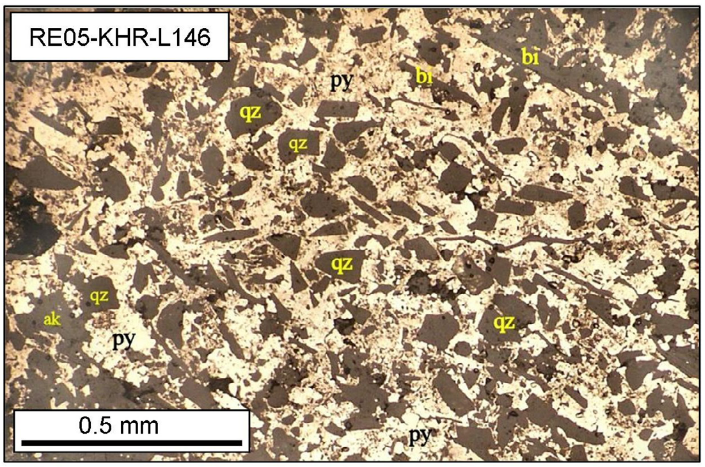

c)

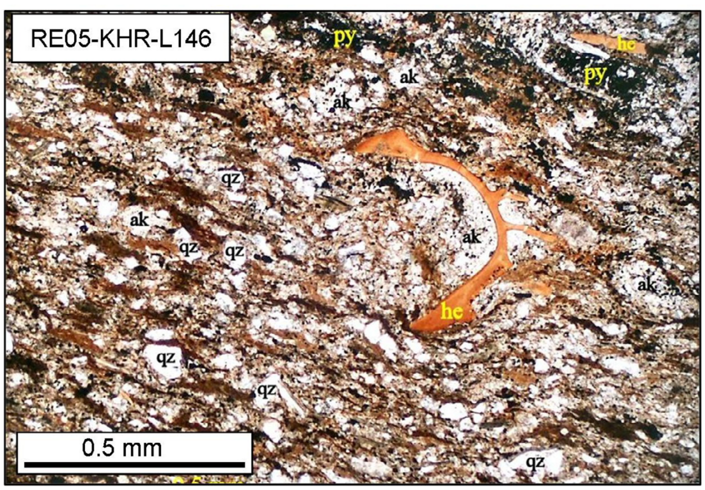

Figure 5. Photomicrographs of sample L146: a) band A comprises ankerite (mainly stained orange by limonite) with disseminated pyrite, band B comprises ankerite with detrital grains of quartz, slender flakes of biotite and minor patches of pyrite (plane-polarized light); b) band C comprises a pyrite network with detrital grains of quartz and flakes of biotite, and lesser grains of ankerite (reflected light); c) band G comprises detrital grains of quartz in a groundmass of cryptocrystalline mudstone with patches of ankerite, lenses containing abundant disseminated pyrite, and a few patches of amorphous hematite, including replacement of organic material (plane-polarized light). Abbreviations: ak, ankerite; bi, biotite; he, hematite; li, limonite; py, pyrite; qz, quartz.

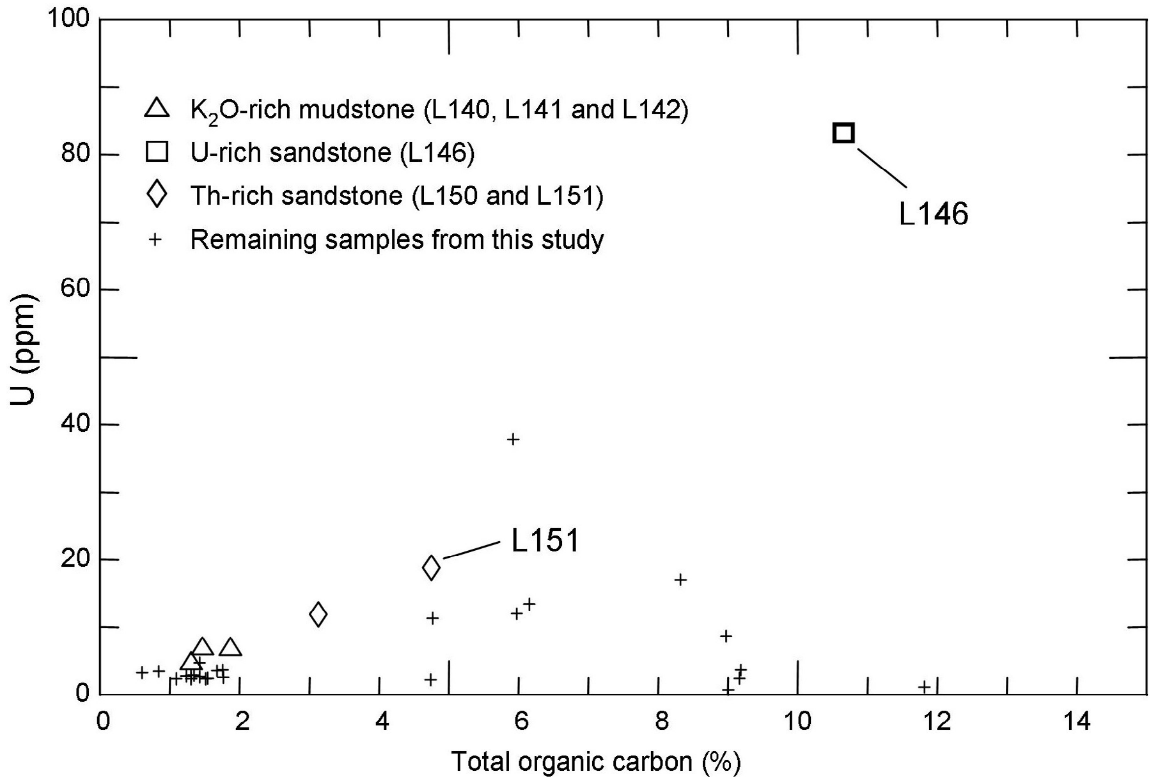

Figure 6. Uranium versus total organic carbon for samples from drillhole BHH04-KHR-02.

A second U-log spike at approximately 102–103 m depth correlates with sample L151, which has 18.8 ppm U. On Figure 6, sample L151 does not exhibit the same high values of U and TOC as sample L146, suggesting that the relationship between U and organic matter evident in sample L146 cannot be the cause for the elevated U in sample L151. Rather, the second U-log anomaly (and sample L151) also coincides with an elevated Th-log anomaly (Figure 4) and, as such, is discussed in more detail below.

4.3 Whole-Rock Geochemical Observations Associated with the Th-log Geophysical Anomaly

Samples L150 and L151, which were obtained from depths of 103.4 and 103.6 m, have the highest Th contents of all BHH-KHR-2 core samples (35.8 and 95.5 ppm, respectively) and correlate with the Th-log anomaly (Figure 4). Sample L150 consists of dark grey silty mudstone with specks of white Fe-sulphate similar in appearance to the sand-sized fecal pellets that form the coccoliths and coccospheres of the Second White Specks Formation shale. Palynological interpretation, however, has ruled out the possibility of First or Second White Specks formations in BHH04-KHR-02 because these strata are missing due to a depositional hiatus extending from Turonian to Santonian (Sweet et al., work in progress, 2009). Similar fine-grained white crystals were separated from Late Cretaceous shale in the High Level area of northwestern Alberta and found by X-ray diffraction to consist of 70% szomolnokite ($FeSO_4•H_2O$), 10% rozenite ($FeSO_4•4H_2O$), 15% gypsum ($CaSO_4•2H_2O$) and 5% pyrite (FeS_2; G. Prior, pers. comm., 2005).

Sample L151 is coarse-grained, Fe-stained sandstone. X-ray diffraction analysis shows that it consists of quartz, gypsum, rozenite, posnjakite ($Cu_4SO_4(OH)_6•2H_2O$) and pyrite, all of which have similar mineralogy to the white speckled crystals identified by Prior (*see* above). The X-ray diffraction analysis also identified muscovite, phlogopite and apatite (Appendix 2). Muscovite is present in most of the samples discussed in this report (Appendix 2), but this is the first appearance of phlogopite and apatite, which are common in ultramafic rocks (i.e., kimberlite). Furthermore, apatite could result in elevated levels of Th; for example, apatite-rich kimberlite dikes from the Bellsbank region of South Africa have particularly high Th (630–920 ppm; Fesq et al., 1975). Ultramafic rocks from the northern Alberta kimberlite province average between 26 and 97 ppm (Eccles, 2004). Thus, it is possible that the Th anomaly might be explained by the presence of apatite in sample L151.

Geochemically, samples L150 and L151 have steeply dipping chondrite-normalized REE patterns with light REE-enrichment up to 1434 times chondrite and heavy REE depletion (La_n/Yb_n ratios of 124 and 264; Figure 3a). Their REE patterns are similar to those of kimberlitic rocks from northern Alberta. This observation is supported by their enrichment in elements of ultramafic affinity (Mg, Co, Ni, Cr) and in incompatible elements (e.g., light REE, P, Nb), the same elements that give kimberlite its characteristic geochemical signature. Table 3 gives the concentrations of these elements in samples L150 and L151, together with selected kimberlite samples from previous whole-rock geochemical analyses of Buffalo Head Hills kimberlite (Eccles, 2004). With the exception of MgO, L150 and L151 are generally comparable, or have compositions of higher kimberlite affinity than the comparative Buffalo Head Hills kimberlite data (Table 3). For example, sample L151 has higher Nb, La, Ce, Ni and Co (392.0, 526.4, 965.7, 7387 and 164.5 ppm, respectively) than the Buffalo Head Hills kimberlite samples. Perhaps low MgO versus high immobile element compositions are caused by depletion and enrichment of soluble and immobile elements, respectively, in the extra-crater–sedimentary-rock setting? Regardless, based on X-ray diffraction and geochemical evidence, samples L150 and L151 should be referred to as kimberlitic mudstone and kimberlitic sandstone, respectively. That is, sedimentary rocks at this horizon have been influenced either by syndepositional kimberlite volcanism or by kimberlitic fluids moving intrusively through the sedimentary strata.

Table 3. Selected geochemical data for the Th-log gamma-ray anomaly samples L150 and L151, with the average composition of the remaining sedimentary rock samples analyzed in this study and Buffalo Head Hills kimberlite compositions for comparison.

Sample	MgO (wt. %)	P_2O_5 (wt. %)	Cr_2O_3 (wt. %)	Nb (ppm)	Sr (ppm)	La (ppm)	Ce (ppm)	Pr (ppm)	Ba (ppm)	Ni (ppm)	Co (ppm)	La/Yb
RE05-KHR-L150	6.1	5.7	6.7	118.6	1032.1	296.4	653.9	64.5	394.5	2409.7	138.6	124.0
RE05-KHR-L151	5.7	3.0	1.2	392.0	1176.9	526.4	965.7	83.8	890.5	7387.4	164.5	264.0
Average of remaining sedimentary rock samples collected in this study												
n=29	2.7	0.4	0.0	10.9	349.4	32.5	63.5	7.5		85.9	14.7	11.8
Comparative kimberlite compositions												
4A-02 (1)	27.6	0.1	0.1	23.1	239.5	13.1	25.2	2.3	133.0	498.0	39.2	126.5
4B-01 (1)	42.8	0.3	0.2	44.7	417.4	50.3	89.3	8.1	356.0	1325.0	95.4	178.9
4C-01 (1)	38.8	0.3	0.1	93.2	216.9	50.9	104.6	9.1	157.0	924.0	67.6	202.3
14-01 (1)	34.8	0.4	0.1	133.0	624.3	141.3	283.4	27.4	308.0	1280.0	86.9	247.9
14B-03 (1)	37.2	0.4	0.1	117.1	336.8	118.4	232.6	22.8	387.0	1340.0	100.1	227.7
14C-06 (1)	29.1	0.5	0.1	158.3	737.3	163.7	312.5	31.0	535.0	1279.0	87.3	282.2
14C-06 (1)	29.3	0.5	0.2	172.5	773.7	176.4	341.8	33.7	559.0	1280.0	91.4	280.0
K14 surface trench (1)	31.3	0.5	0.2	147.2	1162.3	159.9	313.7	30.3	944.0	1206.0	80.7	249.8
BHH average (2)	29.8	0.4	0.1	134.4	645.3	127.2	237.9	22.9	926.2	993.4	78.0	214.0

(1) Geochemical results from Eccles (2004); sample numbers refer to Buffalo Head Hills K4 and K14 kimberlite drill holes

(2) Average compositions of 30 whole rock kimberlite analyses from 16 pipes in the Buffalo Head Hills (Eccles, 2004)

5 Conclusion

A comparison of geochemical data, petrographic interpretation and downhole spectral γ-ray anomalies shows that the γ-ray anomalies can be used to identify potential horizons influenced by kimberlitic mineral– and metallic mineral–bearing fluids and rock types.

A positive correlation between U content, TOC and selective to pervasive replacement of organic debris and groundmass by sulphide minerals and hematite suggests that a distinct U-log γ-ray spike corresponds to reduction and accumulation of U and other metallic minerals and pathfinder elements (e.g., Mo, Zn, Hg, Sb and Se) as fluids moved through an organic-rich sedimentary-rock horizon. Future discovery of extensive downhole spectral γ-ray profiles of this nature should be investigated for metallic mineral potential.

This report shows that a combined U- and Th-log γ-ray anomaly corresponds to an horizon of kimberlitic material, based on the presence of elevated abundances and concentrations of minerals (phlogopite and apatite) and elements (Mg, Co, Ni and Cr, and incompatible elements such as light REE, P and Nb) of ultramafic affinity. That is, the sedimentary rocks cored at the anomalous γ-ray horizon have been augmented either by syndepositional kimberlite volcanism or by kimberlitic fluids moving intrusively through the sedimentary strata. In this particular case, the Th-log γ-ray spike might be more diagnostic than U-log γ-ray in determining kimberlite potential because the U-log γ-ray spike could also be related to sulphide-bearing fluids, as discussed above. In contrast, the high Th-log γ-ray spike in this example is more likely to be associated with those carbonate-enriched ultramafic mineral assemblages observed in the northern Alberta kimberlite province.

Given the many oil and gas well logs available for viewing, further investigation of downhole spectral γ-ray surveys is warranted. These data may one day be used, for example, to assess existing well logs for regional diamondiferous kimberlite potential in Alberta. Other potential uses of downhole γ-ray geophysics include 1) measuring the effectiveness of airborne or ground geophysical exploration programs, 2) identification of rock types that may have been overlooked in the drilling program, and 3) pinpointing the location of lithological core contacts critical to geological modelling.

6 References

Chen, D. and Olson, R. (2005): Regional stratigraphic framework of Buffalo Head Hills–Peerless Lake region, northern Alberta; Alberta Energy and Utilities Board, EUB/AGS Earth Sciences Report 2005-05, 40 p.

Dufresne, M.B., Eccles, D.R. and Leckie, D.A. (2001): The geological and geochemical setting of the mid-Cretaceous Shaftesbury Formation and other Colorado Group sedimentary units in northern Alberta; Alberta Energy and Utilities Board, EUB/AGS Special Report 9, 105 p.

Eccles, D.R. (2004): Petrogenesis of the northern Alberta kimberlite province, M.Sc. thesis, University of Alberta, 179 p.

Fesq, H.W., Kable, E.J.D. and Gurney, J.J. (1975): Aspects of the geochemistry of kimberlite from the Premier mine and other selected South African occurrences, with particular reference to the rare earth elements; Physics and Chemistry of the Earth, v. 9, p. 687–734.

Gromet, L.P., Dymek, R.F., Haskin, L.A. and Korotev, R.L. (1984): The 'North American Shale Composite': its compilation, major and trace element characteristics; Geochimica et Cosmochimica Acta, v. 48, p. 2469–2482.

Hamilton, W.N., Langenberg, W.C., Price, M.C. and Chao, D.K. (1999): Geological map of Alberta; Alberta Energy and Utilities Board, EUB/AGS Map 236, scale 1: 1 000 000.

Hein, F.J. and Eccles, D.R. (2007): Preliminary stratigraphic framework for selected kimberlites in the Buffalo Head Hills region, north-central Alberta, Alberta Energy and Utilities Board, EUB/AGS Geo-Note 2007-02, 40 p.

Klinkhammer, G.P., Elderfield, H., Edmond, J.M. and Mitra, A. (1994): Geochemical implications of rare earth element patterns in hydrothermal fluids from mid-ocean ridges; Geochimica et Cosmochimica Acta, v. 58, p. 5105–5113.

McLennan, S.M. (1989): Rare earth elements in sedimentary rocks: influence of provenance and sedimentary process; *in* Reviews in Mineralogy, B.R. Lipin and G.A. McKay (ed.), Mineralogical Society of America, Washington, D.C., v. 21, p. 169–200.

Michard, A. and Albarede, F. (1986): The REE content of some hydrothermal fluids; Chemical Geology, v. 55, p. 51–60.

Mills, R.A. and Elderfield, H. (1995): Rare earth element geochemistry of hydrothermal deposits from the active TAG Mound, 26ºN Mid-Atlantic Ridge; Geochimica et Cosmochimica Acta, v. 59, p. 3511–3524.

Mwenifumbo, C.J. and Kjarsgaard, B.A. (1999): Gamma-ray logging and radioelement distribution in the Fort à la Corne kimberlite pipe 169; Exploration and Mining Geology, v. 8, p. 137–147.

Pawlowicz, J.G., Fenton, M.M. and Weiss, J.A. (2005): Auger core lithologs, Sawn Lake area, southern Buffalo Head Hills, Alberta; Alberta Energy and Utilities Board, EUB/AGS Geo-Note 2005-07, 48 p.

Skelton, D. and Bursey, T. (1998): Buffalo Head Hills property (AL01), Ashton Mining of Canada Inc; Alberta Geological Survey, Assessment File 19980015, 19 p.

Sun, S.S. and McDonough, W.F. (1989): Chemical and isotopic systematics of oceanic basalts: implications for mantle composition and processes; *in* Magmatism in the Ocean Basins, A.D. Saunders and M.J. Norry (ed.), Geological Society of London, Special Publication 42, p. 313–345.

Toyoda, K. and Masuda, A. (1991): Chemical leaching of pelagic sediments: identification of the carrier of Ce anomaly; Geochemical Journal, v. 25, p. 95–119.

Appendices

Appendix 1. Major and Trace-Element Whole-Rock Geochemistry of Selected Samples from Drillhole BHH04-KHR-02

Sample ID	Downhole γ spike [1]	Drillhole ID	Sample top (m)	Sample bottom (m)	Elevation (m asl)	Lithology	SiO_2 (%)	Al_2O_3 (%)	Fe_2O_3 (%)	MgO (%)	CaO (%)	Na_2O (%)	K_2O (%)	TiO_2 (%)	P_2O_5 (%)	MnO (%)	Cr_2O_3 (%)	Sc (ppm)	LOI (%)	TOT/C (%)	TOT/S (%)	SUM (%)	Be (ppm)	Co (ppm)
RE05-KHR-L121	Negligible	BHH04-KHR-2	13.72	14.20	763.28	Grey mudstone	59.02	15.7	7.05	2.32	1.78	1.05	2.21	0.73	0.28	0.08	0.0134	15	9.7	1.52	0.07	99.94	2	17.7
RE05-KHR-L122	Negligible	BHH04-KHR-2	21.35	21.75	755.65	Grey mudstone	58.81	15.98	6.84	2.33	1.7	0.77	2.44	0.73	0.21	0.05	0.0128	15	9.9	1.77	0.21	99.78	2	13.7
RE05-KHR-L123	Negligible	BHH04-KHR-2	27.43	28.10	749.57	Grey mudstone with silty laminations; trace organics	61.35	15.61	6.27	2.06	1.34	0.59	2.55	0.73	0.21	0.03	0.0136	15	9	1.35	0.4	99.77	3	13.5
RE05-KHR-L124	Negligible	BHH04-KHR-2	31.60	31.60	745.4	Fine-grained, indurated sandstone	61.3	16.02	6.04	2.11	1.21	0.82	2.41	0.76	0.16	0.05	0.0137	14	9	1.31	0.36	99.9	3	15
RE05-KHR-L125	Negligible	BHH04-KHR-2	31.70	32.00	745.3	Carbonate-enriched sandstone	18.85	5.62	5.01	1.41	35.39	0.37	0.74	0.25	0.85	0.11	0.0051	8	31.2	8.98	0.05	99.81	1	5.1
RE05-KHR-L126	Negligible	BHH04-KHR-2	32.00	32.00	745	Grey silty mudstone	61.66	15.57	5.99	2.02	1.74	1.39	2.4	0.7	0.16	0.06	0.0128	13	8.2	1.1	0.55	99.91	2	15.6
RE05-KHR-L127	Negligible	BHH04-KHR-2	32.04	33.80	744.96	Grey silty mudstone	59.08	16.5	6.26	2.38	1.43	0.86	2.24	0.75	0.16	0.05	0.0129	16	10.2	1.31	0.08	99.93	3	14.4
RE05-KHR-L128	Negligible	BHH04-KHR-2	38.11	38.60	738.89	Brown-grey mudstone	58.54	16.18	6.77	2.37	1.78	0.93	2.26	0.74	0.24	0.08	0.0135	17	10	1.55	0.02	99.91	2	16
RE05-KHR-L129	Negligible	BHH04-KHR-2	41.15	43.40	735.85	Grey mudstone with silty laminations	59.64	16.12	6.32	2.36	1.51	0.86	2.42	0.73	0.19	0.05	0.0147	15	9.7	1.43	0.09	99.92	3	16.6
RE05-KHR-L130	Negligible	BHH04-KHR-2	45.72	47.97	731.28	Dark brown silty mudstone	63.83	14.83	5.08	2.01	1.35	0.44	2.7	0.73	0.21	0.02	0.0143	14	8.5	1.68	0.3	99.72	2	12.1
RE05-KHR-L131	Negligible	BHH04-KHR-2	54.80	54.85	722.2	Grey to dark grey mudstone with silty laminations	45.54	8.28	20.95	2.49	3.6	0.39	1.44	0.45	0.63	0.21	0.0092	11	15.8	4.73	0.67	99.79	1	7.7
RE05-KHR-L132	Negligible	BHH04-KHR-2	60.96	61.40	716.04	Brown-grey silty mudstone	66.69	12.85	4.73	2.13	1.85	0.52	2.35	0.68	0.22	0.03	0.0133	12	7.8	1.76	0.25	99.87	1	11
RE05-KHR-L133	Negligible	BHH04-KHR-2	74.65	74.95	702.35	Grey to dark-grey mudstone; silty bioturbated; locally organic-rich	65.97	13.95	4.33	2.09	1.07	0.67	2.34	0.7	0.15	0.02	0.0125	13	8.4	1.24	0.25	99.7	2	14.4
RE05-KHR-L134	Negligible	BHH04-KHR-2	77.72	78.82	699.28	Interlayered dark grey silty mudstone and grey mudstone	65.73	13.9	4.54	1.95	0.77	0.67	2.51	0.72	0.14	0.02	0.0132	14	8.9	1.43	1	99.87	2	14.6
RE05-KHR-L135	Negligible	BHH04-KHR-2	82.30	82.34	694.7	Carbonate-enriched sandstone (concretion?)	20.45	4.82	1.81	2.28	36.58	0.22	0.95	0.25	0.36	0.07	0.0049	7	32	9.14	0.54	99.79	2	5.9
RE05-KHR-L136	Negligible	BHH04-KHR-2	86.90	87.40	690.1	Grey massive mudstone; some organic material	65.1	14.91	5.67	2.01	0.5	0.66	2.79	0.76	0.13	0.05	0.0139	14	7.3	0.61	1.26	99.91	2	19.1
RE05-KHR-L137	Negligible	BHH04-KHR-2	88.54	88.59	688.46	Carbonate-enriched sandstone (concretion?)	17.58	4.72	2.36	2.32	37.4	0.21	0.91	0.23	0.82	0.21	0.005	6	33	9.16	0.98	99.77	<1	6
RE05-KHR-L138	Negligible	BHH04-KHR-2	91.44	92.00	685.56	Grey to dark grey poker-chip mudstone; smectitic?	61.71	16.23	6.65	1.94	0.74	0.6	3.22	0.84	0.18	0.03	0.0169	16	7.7	0.85	1.95	99.86	2	19.5
RE05-KHR-L139	Negligible	BHH04-KHR-2	92.48	92.48	684.52	Carbonate-enriched sandstone (concretion?)	16.63	4.4	2.79	2.15	38.44	0.33	0.89	0.23	2.68	0.37	0.005	13	30.8	8.95	1.3	99.72	<1	7.4
RE05-KHR-L140	K_2O	BHH04-KHR-2	95.11	95.50	682	Dark grey mudstone (note: core problems)	60.42	17.26	5.9	1.99	0.7	0.54	3.36	0.84	0.18	0.03	0.0175	17	8.6	1.31	1.49	99.85	2	14.6
RE05-KHR-L141	K_2O	BHH04-KHR-2	96.01	96.50	681	Grey, blocky mudstone	60.85	16.57	6.19	1.99	0.56	0.56	3.31	0.83	0.24	0.03	0.0177	17	8.7	1.47	1.83	99.85	2	16.5
RE05-KHR-L142	K_2O	BHH04-KHR-2	97.54	98.20	679	Grey mudstone at transition to organic-rich black mudstone	60.33	16.79	5.38	2.02	0.66	0.54	3.24	0.77	0.18	0.03	0.0171	16	9.9	1.87	1.3	99.86	3	13.1
RE05-KHR-L143	Negligible	BHH04-KHR-2	98.20	98.60	678.8	Grey blocky mudstone with silty mudstone laminations	44.59	15.96	7.76	1.74	1.59	0.71	1.66	0.44	0.51	0.02	0.0053	8	21.8	5.91	5.8	96.8	3	17.1
RE05-KHR-L145	Negligible	BHH04-KHR-2	98.65	99.00	678.16	Grey blocky mudstone with silty mudstone laminations	43.78	14.11	5.85	3.05	11.85	0.73	1.36	0.44	0.26	0.09	0.0024	4	18.2	4.76	3.19	99.73	1	12.4
RE05-KHR-L146	U spike	BHH04-KHR-2	99.00	99.06	678	Interbedded carbonate-enriched sandstone and bituminous mudstone	32.45	10.11	6.8	1.09	14.09	0.67	1.64	0.33	1.24	0.08	0.0076	11	21.5	10.66	5.53	90.02	1	19.1
RE05-KHR-L147	Negligible	BHH04-KHR-2	99.06	99.20	677.8	Black, organic-rich mudstone	42.59	11.93	6.04	1.68	13.32	0.41	2.12	0.49	0.14	0.03	0.0106	10	21	8.3	3.71	99.77	1	14.9
RE05-KHR-L148	Negligible	BHH04-KHR-2	99.20	100.00	676.42	Black, organic-rich mudstone	47.18	13.59	6.49	2.67	7.57	0.59	1.9	0.47	0.17	0.02	0.0103	9	18.9	6.14	3.86	99.57	3	16.5
RE05-KHR-L149	Negligible	BHH04-KHR-2	100.58	102.11	674.69	Black, organic-rich mudstone	48.68	13.11	9.29	2.3	1.19	0.68	2.29	0.52	0.14	0.02	0.0125	11	21.2	5.96	6.28	99.44	3	23.2
RE05-KHR-L150	Th spike	BHH04-KHR-2	103.41	103.46	674	Silty mudstone with white iron-sulphates	20.22	7.08	23.24	6.06	8.61	0.23	1.15	0.69	5.65	0.19	6.7354	31	19.3	3.13	12.06	99.28	1	138.6
RE05-KHR-L151	Th spike	BHH04-KHR-2	103.55	103.60	673	Coarse-grained, Fe-stained sandstone (regolith appearance)	9.4	2.81	27.03	5.7	9.84	0.2	0.58	0.78	2.98	0.31	1.1883	35	25.6	4.75	27.74	86.49	2	164.5
RE05-KHR-L152	Negligible	BHH04-KHR-2	104.30	104.40	672.7	Coarse-grained, fractured sandstone; possible bentonite at end of hole	7.05	0.2	3.82	20.05	27.38	0.06	0.05	0.05	0.23	0.09	0.0921	2	40.5	11.78	1.05	99.66	<1	34.1

[1] K_2O, U and Th spikes relate to drill hole BHH04-KHR-02 down hole geophysical (gamma) anomalies

[2] $Ce/Ce^* = Ce_n/(4La_n + Sm_n)$ Toyoda and Masuda (1991):

[3] $Eu/Eu^* = Eu_n/(0.67Sm_n + 0.33Tb_n)$ McLennan (1989):

Sample ID	Cs	Ga	Hf	Nb	Rb	Sn	Sr	Ta	Th	U	V	W	Zr	Y	La	Ce	Pr	Nd	Sm	Eu	Gd	Tb	Dy	Ho	Er	Tm	Yb	Lu	Ba	Mo	Cu	Pb	Zn	Ag
	(ppm)	(ppm)	(ppm)	(ppm)	(ppm)	(ppm)	(ppm)	(ppm)	(ppm)	(ppm)	(ppm)	(ppm)	(ppm)	(ppm)	(ppm)	(ppm)	(ppm)	(ppm)	(ppm)	(ppm)	(ppm)	(ppm)	(ppm)	(ppm)	(ppm)	(ppm)	(ppm)	(ppm)	(ppm)	(ppm)	(ppm)	(ppm)	(ppm)	(ppm)
RE05-KHR-L121	4.6	17.3	4	7.9	66.8	2	157.8	0.6	5.5	2.5	151	1	112.3	23.8	22.4	45.1	5.36	20.6	4.6	1.22	4.13	0.71	3.71	0.81	2.52	0.34	2.1	0.35	630.9	1.5	51	14.2	134	0.2
RE05-KHR-L122	5.5	18.7	3.7	9.5	86.6	1	162.7	0.8	6.8	2.7	175	1.3	125.8	25	24.9	51.4	6.08	23.6	5.3	1.34	4.33	0.73	3.97	0.79	2.51	0.38	2.24	0.38	661.8	1.4	49.5	15.4	144	0.2
RE05-KHR-L123	7.6	18.1	4.3	11.8	106	2	166.2	0.8	8.3	3	195	1.2	134	26.4	31.3	60.4	7.25	27.3	5.8	1.36	4.62	0.8	4.35	0.88	2.66	0.41	2.46	0.42	834.8	1.7	39.6	18.4	159	0.1
RE05-KHR-L124	6.1	18.1	4.5	10.1	84.4	2	174	0.7	5.9	3	172	1.3	130.3	23	26	52.1	6.08	22.6	4.8	1.28	4.15	0.74	3.89	0.83	2.47	0.37	2.56	0.38	847.3	1.8	46.6	16.2	147	0.2
RE05-KHR-L125	1.9	6.1	1.3	3	25.9	<1	388.9	0.2	2.1	0.9	59	0.4	47.2	11.2	9	17.8	2.14	9.5	1.7	0.6	1.86	0.28	1.68	0.35	1.03	0.17	0.94	0.15	689	0.8	18.8	5.4	44	0.1
RE05-KHR-L126	3.8	17.5	4.3	7.9	65.8	<1	240	0.6	5.9	2.5	126	1	125.3	20.8	21.5	44.2	5.24	20.6	4.7	1.25	3.7	0.68	3.57	0.71	2.08	0.36	2.12	0.33	816	1.8	44.7	14.7	125	0.2
RE05-KHR-L127	4.7	19.8	4	8.6	75.5	1	185.7	0.7	6.8	2.5	161	1.2	126.5	22	21.8	44.9	5.57	21.7	4.7	1.29	4.05	0.73	4.07	0.75	2.45	0.35	2.23	0.36	601.6	1.3	56.1	15	140	0.2
RE05-KHR-L128	4.8	19.5	4	8.9	76.3	1	213.2	0.7	6.2	2.6	156	1.3	118.3	25.8	23.9	49.6	6	24.4	5.1	1.4	4.51	0.84	4.4	0.85	2.67	0.43	2.49	0.39	643.3	1.5	59.4	16.6	142	0.2
RE05-KHR-L129	5.9	20	4.2	9.7	86.9	1	206.7	0.7	7.1	2.8	164	2.1	123.5	24.5	25.3	51	6.15	23.4	5.3	1.44	4.02	0.75	4.14	0.81	2.43	0.39	2.29	0.34	727.9	1.4	49.2	16	143	0.2
RE05-KHR-L130	8.9	18.9	4.8	13.1	123.5	2	173.2	1	11.2	3.7	228	2.1	147.4	28.2	36.5	69.5	8.25	30.6	6.2	1.51	4.95	0.88	4.55	0.95	2.84	0.46	2.85	0.4	1101.7	1.5	32.4	19.8	159	0.1
RE05-KHR-L131	4.2	10.1	4.2	7.7	61	1	209	0.6	4.4	2.4	123	1.1	132.5	24.9	22.6	42.6	5.1	19.8	3.9	1.07	3.56	0.6	3.61	0.75	2.31	0.33	1.97	0.37	767.4	1	20.7	10.1	87	0.1
RE05-KHR-L132	6.6	16.5	6	12.2	101.6	2	162.3	0.9	7.8	3.8	187	1.7	189.1	27	33	62	7.41	28	5.3	1.38	4.61	0.84	4.53	0.94	2.79	0.43	2.57	0.45	971.6	1.7	29.8	16.8	143	0.2
RE05-KHR-L133	7.6	17.1	5.2	12.5	107.8	3	270.7	1	9.8	2.9	183	1.6	165.9	27.1	31.7	62.5	7.3	28	5.3	1.72	4.6	0.89	4.55	0.97	2.75	0.45	2.56	0.41	2451.5	1.6	35	17.7	148	0.2
RE05-KHR-L134	8.4	18.8	5.1	13.9	114.8	2	348.7	1	11.7	4.9	205	1.6	183	34	38.4	73.8	8.79	32.9	6.9	1.7	5.54	0.95	5.43	1.2	3.51	0.53	3.28	0.56	844.5	3.4	45.8	19.1	148	0.2
RE05-KHR-L135	3.3	6.4	1.8	5.8	43.8	<1	572.3	0.3	3.6	2.6	71	0.4	59.8	36.2	23.5	42.4	5	18.5	4.5	1.12	4.31	0.75	4.7	1.15	3.58	0.59	3.61	0.6	518	0.9	10.6	7	49	0.1
RE05-KHR-L136	8.4	18.9	5.5	14.7	123.7	2	150.9	1	8.6	3.4	213	1.8	173.7	30.4	36.8	73.1	8.55	33	6.2	1.58	5	0.89	5.25	0.98	3.15	0.48	2.93	0.53	837.6	1.3	28.3	18.8	140	0.1
RE05-KHR-L137	2.9	5.9	1.4	4.2	40.9	<1	784.9	0.2	2.4	3.8	77	0.9	43.6	24.6	17.1	30.8	3.54	14.1	2.8	0.77	3.11	0.48	2.91	0.64	2.07	0.34	1.95	0.32	535.9	1.1	10.7	6.3	43	0.1
RE05-KHR-L138	10.2	20.2	4.8	16.1	142	1	159.6	1	10.5	3.6	278	2.7	162.4	31.7	40.7	79.8	9.43	35.7	7.1	1.72	5.49	1.01	5.12	1.07	3.3	0.53	3.21	0.5	952	1.1	38	21	170	0.1
RE05-KHR-L139	2.8	5.9	1.3	4	40	<1	1136	0.4	2.4	8.8	72	0.7	47.4	53.1	26.7	51.8	6.74	28.8	6.4	1.82	7.44	1.29	7.24	1.6	4.66	0.71	4.18	0.7	633.4	0.9	8.6	6.1	40	0.1
RE05-KHR-L140	12.2	23	4.5	15.6	152.6	2	160.9	1.2	12.4	4.6	313	1.8	143.3	32.2	44.1	81.7	9.78	35.6	7	1.72	5.71	0.97	5.38	1.13	3.27	0.5	3.21	0.52	1035.4	1.4	39.1	20.8	171	0.1
RE05-KHR-L141	10.9	23.4	4.5	15.2	150.6	2	159.6	1	11.8	6.8	294	1.7	142.5	35.6	43.4	82.4	9.84	38.2	7.6	2.02	6.36	1.1	5.82	1.23	3.63	0.57	3.63	0.54	1001	3.3	44.1	21	178	0.2
RE05-KHR-L142	10.7	21.9	4.4	15	143.4	2	154.6	1.2	10.2	6.7	291	2	149.4	28.6	43.6	79.3	9.55	35	7.1	1.56	5.22	0.87	5.09	0.96	2.92	0.46	2.91	0.46	983.6	4.9	47.5	19	167	0.2
RE05-KHR-L143	1.8	17.1	5.7	16.7	39	1	278.6	1	11.2	37.8	278	1.7	156.5	60.8	63.2	142.8	16.81	64	13.1	1.5	12.4	2.02	10.52	2.05	6.29	0.95	5.37	0.83	23534.9	111.3	59	24.4	297	0.5
RE05-KHR-L145	1.2	17.2	4.6	8	34.9	1	256.8	0.8	4.7	11.4	371	0.6	132.7	28.6	31.7	67.2	7.74	29.3	6.5	1.12	5.83	0.91	5.02	1.07	2.84	0.5	2.54	0.39	987.5	62.6	29.4	26.9	180	0.3
RE05-KHR-L146	3	14.2	3.1	8.3	51.5	<1	461.2	0.6	7.6	83.2	370	0.8	119.1	99.6	83.5	151	19.49	79.5	16.6	4.01	18.46	2.69	14.68	2.94	7.82	1.14	6.41	0.91	7366.5	158.7	65.2	17.6	388	0.7
RE05-KHR-L147	6.2	13.6	2.8	9.9	84.4	<1	288.9	0.7	4.7	17.1	346	1.1	90.6	24.2	28.8	56.4	6.47	24.5	4.8	1.1	4.1	0.65	3.92	0.81	2.29	0.33	2.25	0.35	687.4	88.3	49.4	16.7	221	0.4
RE05-KHR-L148	5.3	16.1	3.5	8.9	75	<1	421.9	0.8	9.9	13.5	407	1.3	107.2	20.8	25.6	52.4	5.87	22.1	4.4	0.81	3.72	0.57	3.18	0.67	2.05	0.34	1.95	0.29	1997.7	73.6	48.1	23.1	215	0.4
RE05-KHR-L149	6.1	15	3.7	11	91.2	1	394.8	0.8	8.6	12.1	474	1.6	120.5	24	29.2	60.2	6.99	24.7	4.9	1.01	4.22	0.77	3.8	0.8	2.38	0.36	2.58	0.33	3077.7	81.4	64.4	23.9	262	0.6
RE05-KHR-L150	1.5	11.7	54.3	118.6	44	2	1032.1	12.2	35.8	11.9	437	0.5	1988.5	25.9	296.4	653.9	64.53	205.6	23.8	5.8	12.39	1.57	6.54	0.92	2.07	0.28	1.61	0.22	394.5	43.6	23.5	11.8	240	<.1
RE05-KHR-L151	0.6	7.8	9.4	392	25.8	<1	1176.9	30.1	95.5	18.8	154	2.1	354.9	24.9	526.4	965.7	83.79	240.9	24.9	5.88	10.1	1.39	5.21	0.73	1.84	0.24	1.35	0.22	890.5	8	28.3	33.9	113	<.1
RE05-KHR-L152	<.1	0.7	1.1	26.9	2.2	<1	1693.2	1.9	6.1	1.3	10	0.4	54.2	1.3	34.8	63.6	5.44	15	1.6	0.31	0.62	0.11	0.33	<.05	0.12	<.05	0.08	0.01	547.7	0.8	2.8	2.9	20	0.1

[1] K_2O, U and Th spik

[2] $Ce/Ce^* = Ce_n /(4La_n$

[3] $Eu/Eu^* = Eu_n /(0.67S$

Sample ID	Ni	Mn	Fe	As	Au	Cd	Sb	Bi	Cr	Mg	Ti	Li	Tl	Hg	Se	Pd	Pt	Ce/Ce* [2]	Eu/Eu* [3]
	(ppm)	(ppm)	(%)	(ppm)	(ppm)	(ppm)	(ppm)	(ppm)	(ppm)	(ppm)	(ppm)	(ppm)	(ppm)	(ppb)	(ppm)	(ppb)	(ppb)		
RE05-KHR-L121	56.8	727	5.08	6	<.1	0.3	1.4	0.2	101.1	1.28	0.454	45.7	0.14	90	0.6	<10	<2	0.178	0.807
RE05-KHR-L122	48.9	459	4.8	10	<.1	0.3	1.4	0.2	103.6	1.32	0.446	58.8	0.14	70	0.7	<10	<2	0.182	0.789
RE05-KHR-L123	50.8	290	4.5	17	<.1	0.2	1.4	0.3	111.4	1.13	0.44	68.1	0.12	71	0.9	<10	<2	0.172	0.731
RE05-KHR-L124	51.6	472	4.37	17	<.1	0.3	1.3	0.3	106.1	1.29	0.47	60.9	0.14	76	0.7	<10	<2	0.179	0.811
RE05-KHR-L125	16.8	925	3.55	23	<.1	0.1	0.5	0.1	34.4	0.67	0.161	16.8	0.09	30	0.3	<10	<2	0.176	1.057
RE05-KHR-L126	47.9	510	4.44	13	<.1	0.3	1.3	0.2	89.4	1.21	0.455	46.5	0.24	97	0.4	<10	<2	0.181	0.821
RE05-KHR-L127	49.8	442	4.57	7	<.1	0.2	1.4	0.2	102.2	1.42	0.483	54.3	0.12	68	0.4	<10	<2	0.182	0.834
RE05-KHR-L128	54.4	672	4.98	6	<.1	0.3	1.5	0.2	109.9	1.49	0.473	54.6	0.14	91	0.6	<10	<2	0.183	0.822
RE05-KHR-L129	53.4	456	4.65	7	<.1	0.2	1.5	0.2	118.3	1.42	0.453	56.5	0.14	70	0.7	<10	<2	0.178	0.843
RE05-KHR-L130	40.1	210	3.76	14	<.1	0.2	1.4	0.3	113.1	1.16	0.424	71.7	0.11	81	1.1	<10	<2	0.171	0.755
RE05-KHR-L131	23.7	1796	15.45	12	<.1	0.2	0.7	0.1	66.7	1.43	0.228	43.5	0.1	77	0.6	<10	<2	0.169	0.835
RE05-KHR-L132	36.5	253	3.65	11	<.1	0.3	1.4	0.2	99.3	1.19	0.389	62	0.09	68	0.8	<10	<2	0.169	0.787
RE05-KHR-L133	43.7	211	3.46	13	<.1	0.2	1	0.3	109	1.3	0.433	55.4	0.08	56	0.7	<10	<2	0.177	0.967
RE05-KHR-L134	35.5	167	3.51	16	<.1	0.6	0.9	0.3	109	1.19	0.434	59.8	0.17	77	2.1	<10	2	0.172	0.769
RE05-KHR-L135	14.9	565	1.42	8	<.1	0.1	0.5	0.1	39.8	1.15	0.146	25.9	0.05	28	0.8	<10	<2	0.161	0.743
RE05-KHR-L136	44.1	415	4.15	22	<.1	0.2	0.8	0.3	106.1	1.08	0.4	85.9	0.12	73	0.6	<10	<2	0.178	0.788
RE05-KHR-L137	19.2	1702	1.75	7	<.1	0.1	0.5	0.1	37.2	1.18	0.134	26.9	0.05	29	0.7	<10	<2	0.162	0.816
RE05-KHR-L138	58.6	287	4.86	22	<.1	0.2	1.3	0.4	132.8	1.09	0.482	105.6	0.1	110	1.4	<10	2	0.176	0.751
RE05-KHR-L139	23.6	2665	1.91	14	<.1	0.1	0.5	0.1	32.5	0.91	0.12	25.3	0.08	40	1	<10	<2	0.170	0.808
RE05-KHR-L140	53.8	258	4.21	16	<.1	0.3	1.7	0.3	136.5	1.03	0.463	105.5	0.1	107	2.9	<10	<2	0.167	0.766
RE05-KHR-L141	55.9	243	4.22	22	<.1	0.8	1.6	0.4	136.5	1.06	0.462	100.3	0.27	113	3.8	<10	<2	0.170	0.820
RE05-KHR-L142	47.7	220	3.78	15	<.1	0.7	2.2	0.3	129.2	1.02	0.431	97	0.28	93	4.6	<10	<2	0.164	0.702
RE05-KHR-L143	147.4	149	5.72	43	<.1	5.7	7.7	0.3	32.8	0.98	0.306	30.3	1.87	84	18.9	<10	3	0.200	0.348
RE05-KHR-L145	70.4	714	4.11	28	<.1	2.8	5.3	0.4	19.4	1.66	0.32	62.7	1.04	46	10.5	<10	<2	0.188	0.536
RE05-KHR-L146	221.3	654	5.33	38	<.1	10.2	11.4	0.3	60	0.62	0.226	32.1	1.54	143	30.9	<10	6	0.161	0.726
RE05-KHR-L147	94.4	216	4.11	29	<.1	3.7	5.2	0.3	78	0.86	0.299	57.8	0.9	96	16.8	13	3	0.176	0.718
RE05-KHR-L148	90.1	154	4.58	35	<.1	4.5	6.1	0.3	66.4	1.43	0.287	66.3	1.13	94	17.9	<10	3	0.184	0.582
RE05-KHR-L149	208.8	150	6.71	65	<.1	5.8	6.6	0.3	80.2	1.28	0.315	58.8	1.59	142	23	<10	2	0.185	0.624
RE05-KHR-L150	2409.7	1384	16	111	<.1	1	5.1	0.3	>10000	2.98	0.423	17.3	0.84	94	9.3	<10	5	0.205	0.855
RE05-KHR-L151	7387.4	2643	25.15	29	<.1	0.6	2.3	0.1	5630.5	3.28	0.629	15.6	0.56	25	1.1	<10	4	0.173	0.843
RE05-KHR-L152	730.8	745	2.86	3	<.1	0.1	0.1	<.1	217.2	12.24	0.04	6.7	0.05	<5	0.1	<10	<2	0.172	0.677

[1] K_2O, U and Th spik

[2] $Ce/Ce^* = Ce_n /(4La_n$

[3] $Eu/Eu^* = Eu_n /(0.67S$

Appendix 2. X-Ray Diffractogram for Selected Samples from Drillhole BHH04-KHR-02

Page 19: Appendix 2a – X-ray diffractogram for sample RE05-KHR-L140 (K-log anomaly).

Page 20: Appendix 2b – X-ray diffractogram for sample RE05-KHR-L141 (K-log anomaly).

Page 21: Appendix 2c – X-ray diffractogram for sample RE05-KHR-L142 (K-log anomaly).

Page 22: Appendix 2d – X-ray diffractogram for sample RE05-KHR-L146 (K-log anomaly).

Page 23: Appendix 2e – X-ray diffractogram for sample RE05-KHR-L150 (K-log anomaly).

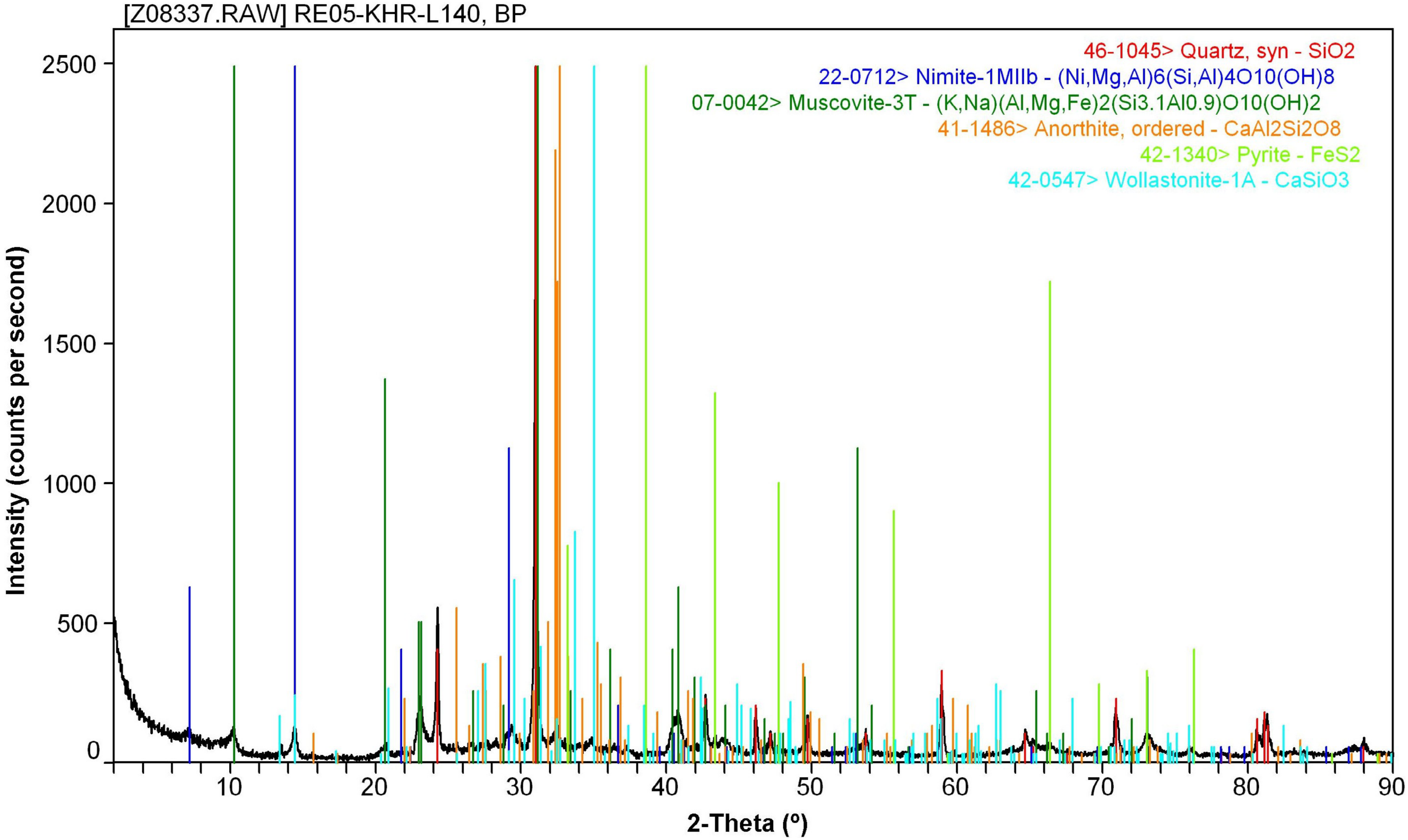
[Z08337.RAW] RE05-KHR-L140, BP
46-1045> Quartz, syn - SiO2
22-0712> Nimite-1MIIb - (Ni,Mg,Al)6(Si,Al)4O10(OH)8
07-0042> Muscovite-3T - (K,Na)(Al,Mg,Fe)2(Si3.1Al0.9)O10(OH)2
41-1486> Anorthite, ordered - CaAl2Si2O8
42-1340> Pyrite - FeS2
42-0547> Wollastonite-1A - CaSiO3
Intensity (counts per second)
2500
2000
1500
1000
500
0
10
20
30
40
50
60
70
80
90
2-Theta (º)

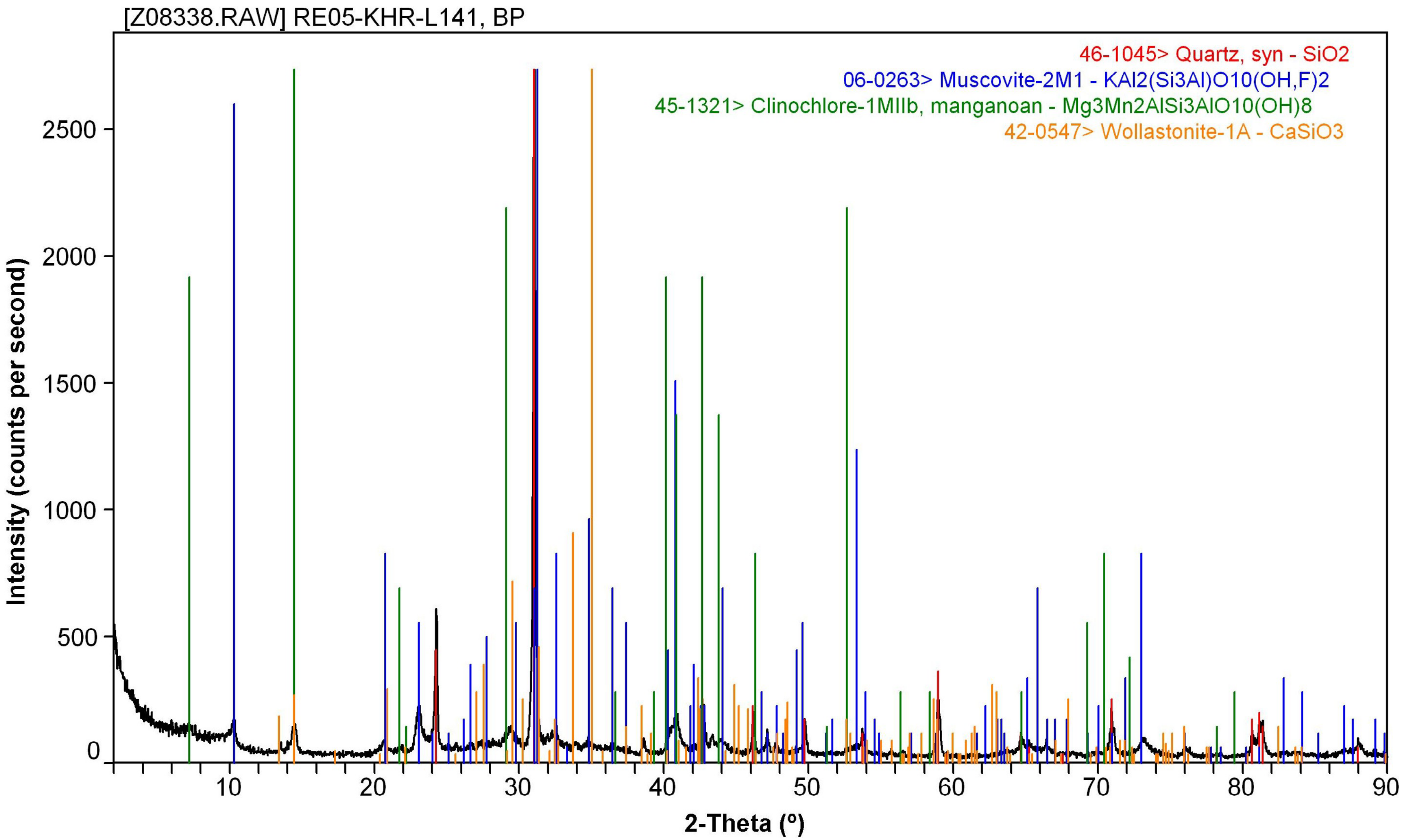
[Z08338.RAW] RE05-KHR-L141, BP
46-1045> Quartz, syn - SiO2
06-0263> Muscovite-2M1 - KAl2(Si3Al)O10(OH,F)2
45-1321> Clinochlore-1MIIb, manganoan - Mg3Mn2AlSi3AlO10(OH)8
42-0547> Wollastonite-1A - CaSiO3
Intensity (counts per second)
2500
2000
1500
1000
500
0
10
20
30
40
50
60
70
80
90
2-Theta (º)

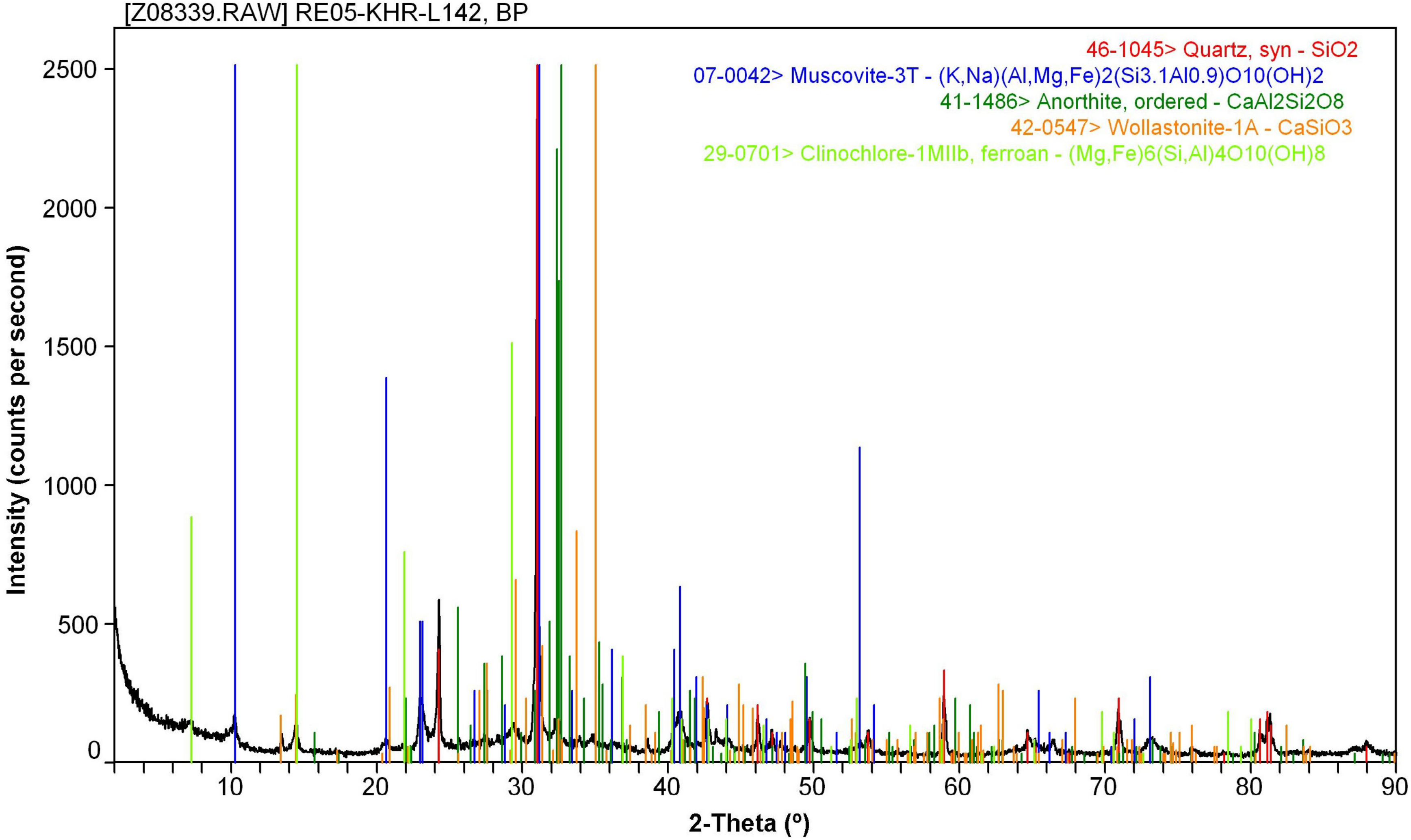
[Z08339.RAW] RE05-KHR-L142, BP
46-1045> Quartz, syn - SiO2
07-0042> Muscovite-3T - (K,Na)(Al,Mg,Fe)2(Si3.1Al0.9)O10(OH)2
41-1486> Anorthite, ordered - CaAl2Si2O8
42-0547> Wollastonite-1A - CaSiO3
29-0701> Clinochlore-1MIIb, ferroan - (Mg,Fe)6(Si,Al)4O10(OH)8
Intensity (counts per second)
2500
2000
1500
1000
500
0
10
20
30
40
50
60
70
80
90
2-Theta (º)

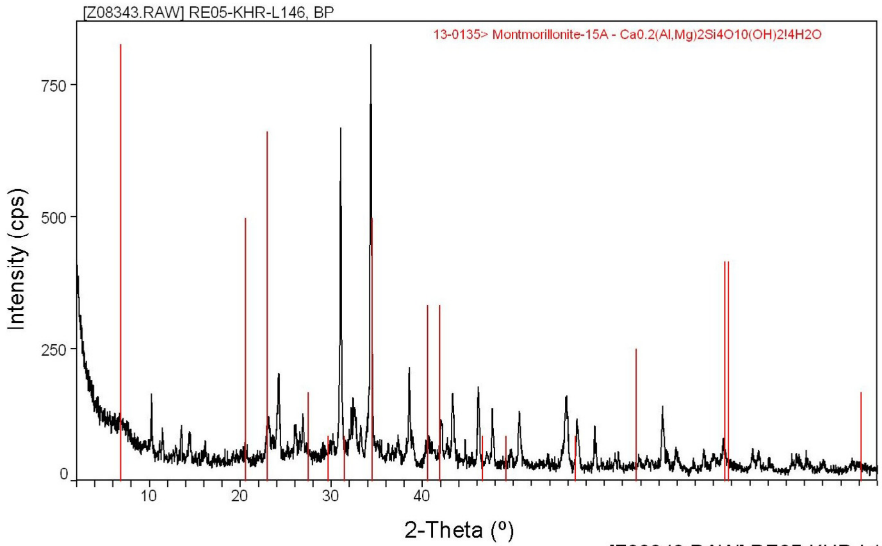
[Z08343.RAW] RE05-KHR-L146, BP
13-0135> Montmorillonite-15A - Ca0.2(Al,Mg)2Si4O10(OH)2!4H2O
Intensity (cps)
750
500
250
0
10
20
30
40
2-Theta (º)

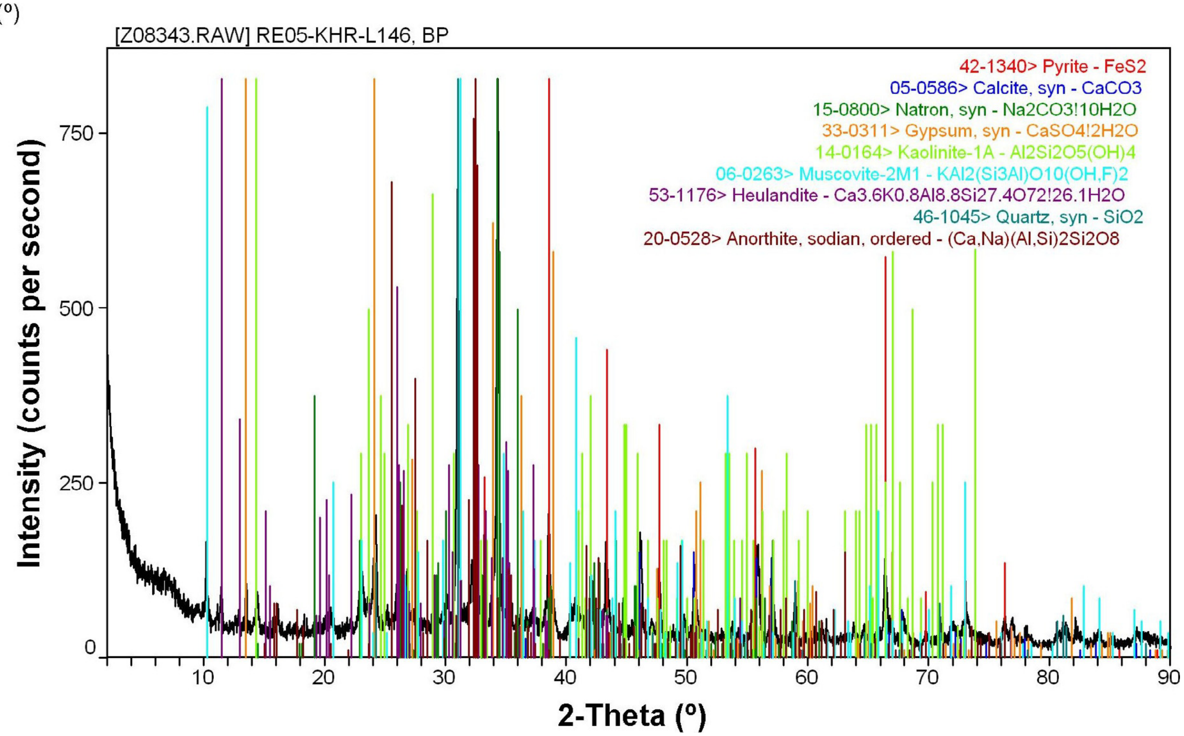
[Z08343.RAW] RE05-KHR-L146, BP
42-1340> Pyrite - FeS2
05-0586> Calcite, syn - CaCO3
15-0800> Natron, syn - Na2CO3!10H2O
33-0311> Gypsum, syn - CaSO4!2H2O
14-0164> Kaolinite-1A - Al2Si2O5(OH)4
06-0263> Muscovite-2M1 - KAl2(Si3Al)O10(OH,F)2
53-1176> Heulandite - Ca3.6K0.8Al8.8Si27.4O72!26.1H2O
46-1045> Quartz, syn - SiO2
20-0528> Anorthite, sodian, ordered - (Ca,Na)(Al,Si)2Si2O8
Intensity (counts per second)
750
500
250
0
10
20
30
40
50
60
70
80
90
2-Theta (º)

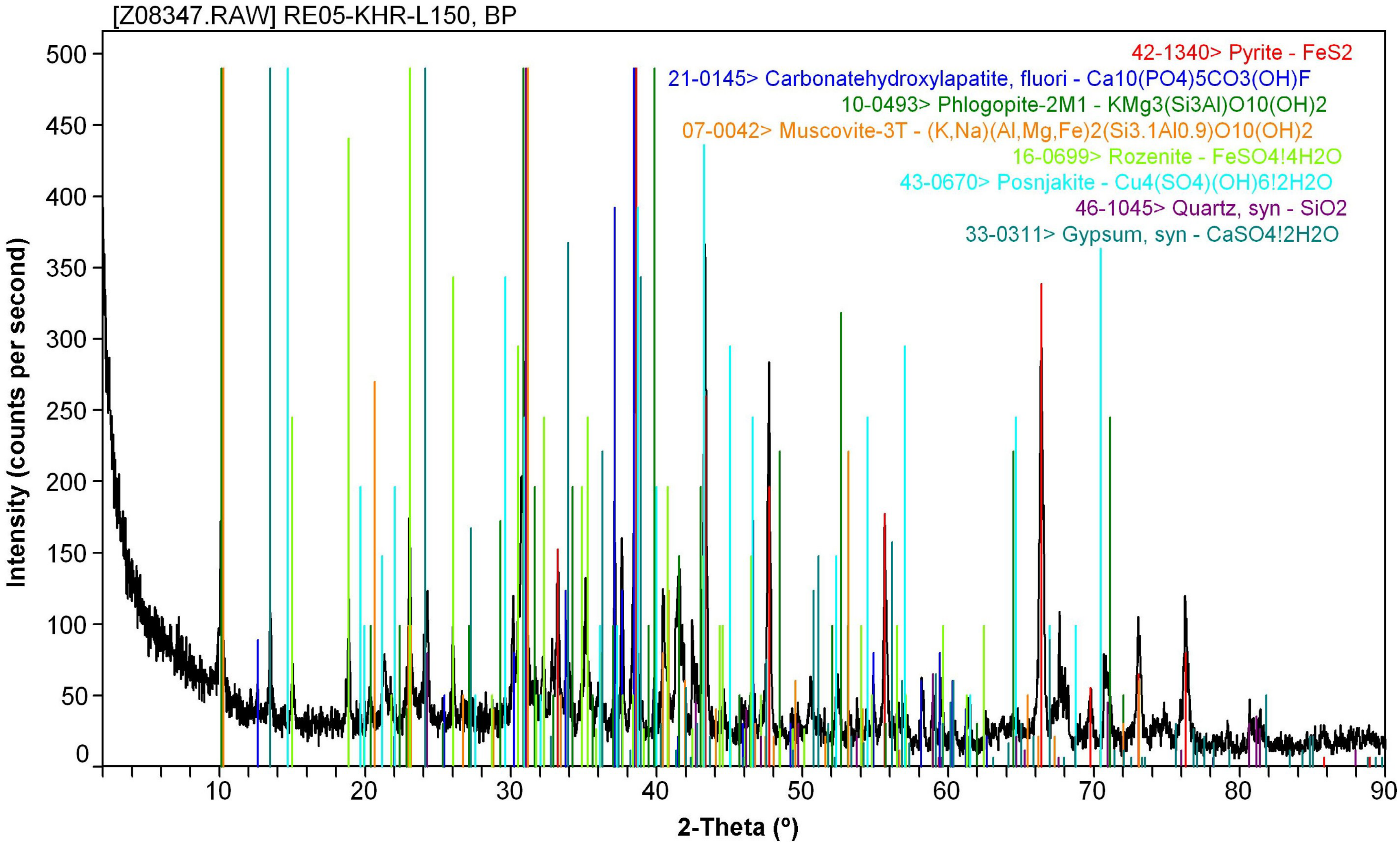
[Z08347.RAW] RE05-KHR-L150, BP
42-1340> Pyrite - FeS2
21-0145> Carbonatehydroxylapatite, fluori - Ca10(PO4)5CO3(OH)F
10-0493> Phlogopite-2M1 - KMg3(Si3Al)O10(OH)2
07-0042> Muscovite-3T - (K,Na)(Al,Mg,Fe)2(Si3.1Al0.9)O10(OH)2
16-0699> Rozenite - FeSO4!4H2O
43-0670> Posnjakite - Cu4(SO4)(OH)6!2H2O
46-1045> Quartz, syn - SiO2
33-0311> Gypsum, syn - CaSO4!2H2O
Intensity (counts per second)
2-Theta (°)
0
50
100
150
200
250
300
350
400
450
500
10
20
30
40
50
60
70
80
90